Improved efficacy of cisplatin delivery by peanut agglutinin-modified liposomes in non-small cell lung cancer

BEN YANG[1,2], RONGGUAN KOU[1], HUI WANG[1], ANPING WANG[1], LILI WANG[1], SIPENG SUN[1,2], MENGQI SHI[1], SHOUZHEN ZHAO[1], YUBING WANG[1], YI WANG[1], JINGLIANG WU[1], FEI WU[1], FAN YANG[3], MEIHUA QU[2], WENJING YU[1] and ZHIQIN GAO[1]

[1]School of Life Science and Technology, Shandong Second Medical University, Weifang, Shandong 261053, P.R. China; [2]Translational Medical Centre, Weifang Second People's Hospital, Weifang, Shandong 261041, P.R. China; [3]Department of Research and Development, Shandong Kanghua Biotechnology Co., Ltd., Weifang, Shandong 261057, P.R. China

Received March 6, 2024; Accepted June 5, 2024

DOI: 10.3892/ijmm.2024.5394

Abstract. Globally, non-small cell lung cancer (NSCLC) is a significant threat to human health, and constitutes >80% of lung cancer cases. Cisplatin (CDDP), a commonly used drug in clinical treatment, has been the focus of research aiming to mitigate its potent toxicity through encapsulation within liposomes. However, challenges, such as a reduced drug loading efficiency and nonspecific release, have emerged as obstacles. The present study aimed to improve the encapsulation efficiency of CDDP within liposomes by pre-preparation of CDDP and modifying the liposome surface through the incorporation of peanut agglutinin (PNA) as a ligand [CDDP-loaded PNA-modified liposomes (CDDP-PNA-Lip)]. This strategy was designed to enhance the delivery of CDDP to tumour tissues, thereby reducing associated side effects. The effect of CDDP-PNA-Lip on the proliferation and migration of NSCLC cell lines with high MUC1 expression was elucidated through *in vitro* studies. Additionally, the capacity of PNA modification to augment the targeted anti-tumour efficacy of liposomes was assessed through xenograft tumour experiments. The results indicated that in an *in vitro* uptake assay Rhodamine B (RhB)-loaded PNA-modified liposomes were taken up by cells with ~50% higher efficiency compared with free RhB. In addition, CDDP-PNA-Lip resulted in a 2.65-fold enhancement of tumour suppression *in vivo* compared with free CDDP. These findings suggested that the encapsulation of CDDP within ligand-modified liposomes may significantly improve its tumour-targeting capabilities, providing valuable insights for clinical drug development.

Correspondence to: Mr. Wenjing Yu or Professor Zhiqin Gao, School of Life Science and Technology, Shandong Second Medical University, 7166 Baotong Road, Weifang, Shandong 261053, P.R. China
E-mail: yuwjwf@163.com
E-mail: zhiqingao2013@163.com

Key words: liposomes, cisplatin, MUC1, non-small cell lung cancer

Introduction

Lung cancer remains a leading cause of cancer-related mortality worldwide, with non-small cell lung cancer (NSCLC) accounting for ~85% of all lung cancer cases (1,2) Despite advances in diagnostic and therapeutic strategies, the prognosis for patients with NSCLC remains poor, primarily due to the late-stage diagnosis and the limited efficacy of conventional treatments (3,4). Chemotherapy, particularly with platinum-based drugs such as cisplatin (CDDP), is a cornerstone in the management of NSCLC (5,6). However, the clinical use of CDDP is significantly hampered by its systemic toxicity, poor solubility and the development of drug resistance in tumour cells. These challenges underscore the urgent need for innovative strategies that can enhance the delivery and therapeutic efficacy of CDDP, while minimizing its adverse effects (7).

Advances in nanotechnology have provided promising avenues for the targeted delivery of chemotherapeutic agents. Liposomes, which are spherical vesicles consisting of one or more phospholipid bilayers, have emerged as versatile drug delivery systems due to their biocompatibility, ability to encapsulate both hydrophilic and hydrophobic drugs, and potential for surface modification to achieve targeted delivery (8-10). The encapsulation of CDDP in liposomes has been explored as a strategy to improve its pharmacokinetic profile and reduce its toxicity (11). However, the challenge of specifically directing these liposomal formulations to tumour tissues remains a significant hurdle in maximizing their therapeutic efficacy against NSCLC (12).

The concept of active targeting, which involves the modification of liposomal surfaces with ligands that can specifically bind to receptors upregulated on cancer cells, represents a viable strategy for overcoming this challenge (13-17). MUC1, a membrane-bound mucin, exhibits a unique expression pattern on tumour cells, presenting a targetable epitope (18-20). Peanut agglutinin (PNA), a plant lectin with high affinity for the Thomsen-Friedenreich (TF) antigen, has garnered attention in this context (21,22). Notably, the TF antigen is a core antigenic site of MUC1, which is expressed on the surface of tumour cells, providing conditions for PNA binding, thus making it a

potential target for PNA-modified liposomes (PNA-Lip) (23). The present study aimed to explore the development and evaluation of PNA-Lip for the targeted delivery of CDDP to NSCLC cells. By leveraging the specific binding affinity of PNA to the TF antigen, the study aimed to enhance the accumulation of CDDP in NSCLC tissues, thereby improving its therapeutic efficacy and reducing systemic toxicity. Through a comprehensive investigation encompassing liposome formulation, characterization, *in vitro* cytotoxicity assays and *in vivo* antitumour efficacy analyses, this research may provide a novel and effective approach for the treatment of NSCLC with CDDP-loaded PNA-modified liposomes (CDDP-PNA-Lip).

Materials and methods

Materials. Soy phospholipids (SPC), DPPG, cholesterol (Chol) and DSPE-PEG2K were purchased from AVT (Shanghai) Pharmaceutical Technology Co., Ltd. DSPE-PEG2K-NHS was purchased from Xi'an Ruixi Biological Technology Co., Ltd. PNA was purchased from Medicago AB. CDDP and sulfo-Cyanine7 carboxylic acid (Cy7) were purchased from Dalian Meilun Biology Technology Co., Ltd.

The human lung cancer cell lines A549 (MUC1-high) and H460 (MUC1-low) were purchased from The Cell Bank of Type Culture Collection of The Chinese Academy of Sciences. A549 cells were cultured in Dulbecco's modified Eagle's medium (Dalian Meilun Biology Technology Co., Ltd.) supplemented with 10% heat-inactivated foetal bovine serum (FBS; Biological Industries), 100 U/ml penicillin and 100 μg/ml streptomycin in a humidified atmosphere containing 5% CO_2 at 37˚C. H460 cells were cultured in RPMI 1640 medium (Dalian Meilun Biology Technology Co., Ltd.) supplemented with 10% heat-inactivated FBS, 100 U/ml penicillin and 100 μg/ml streptomycin at 37˚C in a humidified atmosphere containing 5% CO_2. A total of 29 male BALB/C-nu mice (weight, 13-17 g; age, 4-6 weeks) were purchased from Beijing Vital River Laboratory Animal Technology Co., Ltd. The Ethical Review Committee of Shandong Second Medical University (Weifang, China) approved the present study (approval no. 2022SDL448), which complied with institutional animal care guidelines.

The Cancer Genome Atlas (TCGA) analysis of MUC1. The relationship between MUC1 expression and the clinicopathological characteristics of patients with lung cancer was statistically analysed using relevant clinical data from TCGA database (Project Name: Lung Adenocarcinoma; portal.gdc.cancer.gov/projects/TCGA-LUAD), and the figures were generated using GEPIA (gepia.cancer-pku.cn) and cbioportal (cbioportal.org) (24). Imaging data were obtained from the Human Protein Atlas (proteinatlas.org). The present study complies with the National Institutes of Health TCGA Human Guidelines for Subject Protection and Data Access Policy, as well as the proteinatlas.org citation regulations for images.

Dialysis bag pretreatment. Due to the presence of trace amounts of sulphides, heavy metals and some UV-absorbing impurities in the dialysis bags, they need to be pretreated prior to use. Briefly, after the bags were cut to size, they were boiled for 10 min in 2% sodium bicarbonate and 1 mmol/l EDTA (pH 8.0), and 1 mmol/l EDTA (pH 8.0), respectively. The bags were then washed on the inside and outside surfaces with purified water and stored at 4˚C.

DSPE-PEG2K-PNA synthesis. A total of 10 mg PNA was weighed, completely dissolved in PBS (pH 7.4), reconstituted into a PNA solution with a concentration of 5 mg/ml and set aside. Subsequently, 100 μl DSPE-PEG2K-NHS in DMSO solution (100 mg/ml) was added to the PNA solution, and after 4 h of incubation at room temperature, the entire solution was transferred to treated dialysis bags. Dialysis was performed three times using ddH_2O (2 h each time), and DSPE-PEG2K-PNA was obtained after freeze-drying at -60˚C for 24 h. PNA and DSPE-PEG2K-PNA (10 μg) then underwent SDS-PAGE on 12% gels. Subsequently, the gels were stained with 0.25% Coomassie brilliant blue staining solution. After the SDS-PAGE was decolorized with decolorization solution (cat. no. P0017C; Beyotime Institute of Biotechnology) until it was nearly colourless and the bands were clear, the SDS-PAGE mixture was stained with PEG dye to confirm the successful synthesis of DSPE-PEG2K-PNA. The infrared absorption spectra of PNA, DSPE-PEG2K and DSPE-PEG2K-PNA were examined using an infrared absorption spectrometer, and the characteristic peaks of PNA, DSPE-PEG2K and DSPE-PEG2K-PNA were compared to determine the successful synthesis of DSPE-PEG2K-PNA.

Preparation of the pretreated CDDP solution. CDDP pretreatment was performed according to the methods reported by Zahednezhad *et al* (24). According to Le Chatelier's principle, CDDP undergoes a hydration reaction in water to produce $Pt(NH_3)_2Cl_2 + 2\ H_2O \leftrightarrows [Pt(NH_3)_2(H_2O)_2]^{2+} + 2Cl^-$, and the CDDP generated using this derivative approach has a positive charge on its surface, enabling its active loading in liposomes. The product generated by this reaction is the form in which CDDP undergoes active intracellular action, and thus its antitumour effect is not altered (25). A pretreated CDDP solution was prepared by dissolving CDDP in pure water. The solution was then placed in a magnetic stirrer and set at a speed of 150 rpm. The mixture was incubated at 65˚C for 6 h. Finally, the solution was stored in the dark at 4˚C.

Preparation of PNA-modified CDDP-loaded liposomes (CDDP-Lip). Film dispersion was used to create blank liposomes (Lip) (26,27). In a clean round-bottomed flask, the phospholipids needed to make liposomes were measured in accordance with a mass ratio of SPC:DPPG:Chol:DSPE-PEG2K=15:4:15:4 (SPC:DPPG:Chol:DSPE-PEG2K:DSPE-PEG2K-PNA=15:4:15:4:3 for the PNA-modified liposomes). An ultrasonic cell washer was used to sonicate (20 kHz; 20% power at 0˚C; duration, 2 sec) the aforementioned phospholipids to thoroughly dissolve and combine them; a chloroform-methanol ratio of 2:1 was used for this purpose. The chloroform-methanol mixture with dissolved lipid material was then transferred to an eggplant flask and linked to a rotary evaporator (Yamato Scientific Shanghai Corp.). The rotary evaporator speed, water bath temperature and pressure were adjusted so that all the organic solvents were evaporated slowly and uniformly until a homogeneous lipid film was visible to the naked eye, after which the rotary evaporator pressure

was adjusted to the maximum and maintained for >30 min to ensure that all the organic reagents were removed 5 ml ddH_2O was then added to the eggplant bottle, which was submerged in the ultrasonic cell washer for 5 min to ensure that all the lipid films were eluted; the liposomes were hydrated using the rotary evaporator; and after 1 h, the hydrated liposomes were sonicated (20 kHz; 20% power at 0˚C) for 5 min using the probe and filtered three times using 0.45 and 0.22-μm filters. The dialysis bags were removed and completely washed with ethanol on the surface and inside with pure water, and all of the filtered liposomes were then transferred to the washed bags for dialysis. The liposomes were dialyzed using ddH_2O for 6 h to eliminate any phospholipids that did not form liposomes. The water was replaced every 2 h to ensure thorough dialysis. Finally, the liposomes were collected from the dialysis bag and stored at 4˚C.

The method used for the preparation of CDDP-Lip was essentially the same as that aforementioned. Briefly, the formed lipid film was subsequently hydrated with the pretreated CDDP solution at a ratio of 10:1 total phospholipid mass to drug mass, and the hydration time was suitably extended to allow the pretreated CDDP to be well encapsulated by the liposomes, followed by sonication (20 kHz; 20% power at 0˚C; duration, 2 sec) of the CDDP-Lip for 10 min using a probe. CDDP-Lip were obtained by dialysis with ddH_2O three times (2 h each time) and were stored at 4˚C.

Liposomes were labelled with Rhodamine B (RhB) and Cy7 fluorescent probes to study the cellular absorption and biodistribution of the preparations *in vitro* (RhB) and *in vivo* (Cy7) (28-30). The method used for the preparation of Cy7-loaded liposomes (Cy7-Lip) or RhB-loaded liposomes (RhB-Lip) was essentially the same as that aforementioned. Notably, the total mass of phospholipids relative to the mass of the fluorescent marker was 50:1 during hydration and when the fluorescent marker was added and hydrated.

Characterization of liposomes. Several types of liposomes (CDDP-PNA-Lip for electron microscopy; Lip, CDDP-Lip, PNA-Lip and CDDP-PNA-Lip for characterisation measurements) were diluted 10 times with ddH_2O. Subsequently, a transmission electron microscope (TEM; JEOL, Ltd.) was used to examine the samples. Samples were prepared by negative staining with phosphotungstic acid. Briefly, the sample was added dropwise directly onto a copper grid and left to stand at room temperature for 3 min before excess liquid was aspirated. After waiting for the sample to dry completely, 2% phosphotungstic acid was added dropwise, and after 2 min of staining at room temperature, the excess liquid was aspirated, and the sample was left to dry naturally. Using a Malvern Zetasizer Nano ZS 90 (Malvern Panalytical, Ltd.), the ζ potentials and particle size distributions were measured.

High-performance liquid chromatography (HPLC) was used to quantify drug loading (DL) and entrapment efficiency (EE). Briefly, the HPLC was performed using an Agilent 1260 Infinity II system (Agilent Technologies, Inc.), with a column size of 4.6x200 mm packed with Hypersil ODS2 (filler particle size, 5 μm; Dalian Elite Analytical Instruments Co., Ltd.) on a sample size of 20 μl. The mobile phase consisted of a mixture of methanol and water (v/v=75:25) at a flow rate of 1 ml/min, and the column temperature was maintained at 25˚C. The standard was purchased from Shanghai Yuanye Bio-Technology Co., Ltd. (cat. no. B24462), and the peak areas of 100, 75 and 50 μg/ml were measured to determine the standard curve (31). Triton X-100 (0.1%) was applied to quickly release the internal CDDP solution and destroy the CDDP-Lip. After mixing sodium diethyldithiocarbamate (DDTC) and the sample, the mixture was subsequently incubated in a water bath at 37˚C. Afterward, the sample was thoroughly mixed with chloroform, and the complex formed by DDTC and CDDP was extracted and detected. The EE and DL of the CDDP-Lip were calculated using the following formulas:

EE (%) = Mass of the CDDP loaded/Total mass of the CDDP added x100

DL (%) = Mass of the CDDP loaded/Total mass of liposomes x100

Stability analysis and drug release from CDDP-Lip. The stabilities of the liposomes, PNA-liposomes, CDDP-Lip and CDDP-PNA-Lip were investigated by removing liposomes stored in ddH_2O at 4˚C every 2 days for 14 days, and measuring their particle sizes and ζ potentials.

The drug release profiles of CDDP, CDDP-Lip and CDDP-PNA-Lip were measured using *in vitro* dialysis. The CDDP concentrations of the different groups were adjusted to the same level using PBS and then added to the dialysis bags, which were subsequently placed into conical flasks filled with 100 ml PBS. The samples were incubated at 37˚C in a constant temperature shaker at 100 rpm, and the PBS in the conical flask was removed at different time points and replenished to 100 ml with fresh PBS. The cumulative *in vitro* release curves of CDDP were plotted using HPLC, as aforementioned, to determine the CDDP concentration in the samples at different time points, with time as the horizontal coordinate and the cumulative percentage release of CDDP as the vertical coordinate.

Detection of MUC1-positive cells. MUC1-positive cells were detected via western blotting. Briefly, the A549 and H460 cell lines were inoculated into culture dishes and cultured for 48 h in complete medium supplemented with 10% FBS. After the cells were washed with PBS, the proteins were extracted from the remaining cells with protein extraction buffer [50 mM Tris (pH 7.4), 150 mM NaCl, 10 mM $MgCl_2$, 1% Triton X-100 (v/v), 1% sodium deoxycholate (v/v), 0.1% SDS (v/v), 5 mg/ml sodium orthovanadate]. Protein quantification was performed using a BCA assay. Subsequently, proteins (10 μg) were separated by SDS-PAGE (10% resolving gel and 4% stacking gel). The proteins were then transferred to BioTrace nitrocellulose membranes, which were blocked with 5% non-fat dry milk at 37˚C for 1 h. The membranes were then incubated with the MUC1 (D9O8K) XP® Rabbit mAb (1:1,000; cat. no. 14161; Cell Signaling Technology, Inc.) and β-actin antibody as a loading control (1:1,000; cat. no. sc-47778; Santa Cruz Biotechnology, Inc.) overnight at 4˚C, followed by incubation with anti-rabbit IgG and anti-mouse IgG, HRP-linked secondary antibody (1:2,000; cat. nos. 7074S and 7076S; Cell Signaling Technology, Inc.) for 1 h at room temperature. The blots were visualized using WesternBright ECL, (cat. no. 230329-20; Advantsa Inc.) and underwent densitometric analysis using

ImageJ (version 2.9 011.53t; National Institutes of Health). Subsequently, MUC1 expression in the cell lines was detected by western blotting to distinguish between MUC1-positive cell lines and MUC1-negative cell lines.

In vitro cellular liposome uptake assay. The cellular uptake of CDDP-PNA-Lip was simulated by observing the *in vitro* uptake of RhB fluorescent liposomes by A549 and H460 cells through laser confocal microscopy. The targeting efficiency of CDDP-PNA-Lip was evaluated. A549 and H460 cells were seeded at a density of $5x10^5$ cells/dish in Petri dishes suitable for laser confocal microscopy using complete medium supplemented with 10% FBS. The cells were incubated at 37˚C for 24 h. Subsequently, different concentrations of RhB, RhB-Lip and RhB-loaded PNA-modified liposomes (RhB-PNA-Lip) were added to the medium (at a final RhB concentration of 50 μg/ml), and the mixture was incubated for 6 h at 37˚C. Afterwards, the medium was removed, and the cell surface was cleaned using precooled PBS at 4˚C. Subsequently, the cells were fixed with 4% paraformaldehyde for 10 min at room temperature and washed 3-5 times with PBS to remove residual paraformaldehyde and unfixed cells. Next, the cells were treated with 0.1% Triton X-100 for 10 min at room temperature to permeabilize the cell and nuclear membranes, and were washed 3-5 times with PBS until the PBS was clear and foam free. The nuclei were then stained with DAPI staining solution for 10 min at room temperature and washed 3-5 times with PBS to remove any residual DAPI and the samples were finally observed using a laser confocal microscope.

Antitumour efficacy of CDDP and hydrated CDDP in vitro. The cytotoxicity of various drugs was assessed using the MTS assay, and the reaction product was dissolved in DMEM). Briefly, A549 and H460 cells were inoculated into 96-well plates at a density of 5,000 cells/well and were cultured in complete medium for 24 h. Once cell adhesion and extension were observed, various concentrations of CDDP and hydrated CDDP (concentration gradient, 50.00, 25.00, 12.50, 6.25, 3.12, 1.56, 0.78 and 0.39 μg/ml) were added. After incubation for 48 h, the optical density (OD) values were measured using a microplate reader (PerkinElmer, Inc.) at 490 nm. The rate of cell viability was calculated using the following equation: Cell viability (%)=(ODsample-ODblank)/(ODcontrol-OD-blank) x100.

Antitumour efficacy of CDDP-PNA-Lip in vitro. The cytotoxicity of CDDP, CDDP-Lip and CDDP-PNA-Lip was assessed using the MTS assay, and the reaction product was dissolved in DMEM. Briefly, A549 and H460 cells were inoculated into 96-well plates at a density of 5,000 cells/well and were cultured in complete medium for 24 h. Once cell adhesion and extension were observed, various concentrations of drugs (concentration gradient, 50.00, 25.00, 12.50, 6.25, 3.12, 1.56, 0.78 and 0.39 μg/ml) were added. After incubation for 48 and 24 h, the OD values were measured using a microplate reader (PerkinElmer, Inc.) at 490 nm. The rate of cell viability was calculated using the following equation: Cell viability (%)=(ODsample-ODblank)/(ODcontrol-OD-blank) x100.

Detection of apoptosis-inducing effects of CDDP-PNA-Lip in vitro. The percentage of NSCLC cells that underwent apoptosis after various drug treatments was analysed using the FITC Annexin V Apoptosis Assay kit (cat. no. 556547; BD Biosciences). A549 and H460 cells were inoculated into 6-well plates at a density of $3x10^5$ cells/well, cultured in complete medium for 24 h, and were treated with 2.5 μg/ml CDDP, CDDP-Lip or CDDP-PNA-Lip for 48 h at 37˚C. Subsequently, all of the cells were collected and washed twice with precooled PBS at 4˚C. The cells were diluted to $1x10^6$ cells/ml using 1X binding buffer, and were then co-incubated with FITC-conjugated Annexin V and PI (binding buffer:FITC-conjugated Annexin V/PI=20:1, v/v) staining solution for 15 min at room temperature in the dark. Subsequently, the incubation was terminated by the addition of 1X binding buffer, and the cells were analysed using the BD Accuri C6 Plus Flow Cytometer (BD Biosciences) and BD Accuri C6 Plus software (version 1.0.34.1; BD Biosciences).

Detection of antimigratory efficacy of CDDP-PNA-Lip in vitro. The effect of CDDP, CDDP-Lip and CDDP-PNA-Lip treatments on the lateral migration ability of NSCLC cells was examined using a cell scratch wound healing assay. A549 and H460 cells in the logarithmic growth phase were inoculated into separate 6-well plates. Once the cells had grown to cover the entire well, various drugs were added to each well (2.5 μg/ml, with normal saline used as a control) and the medium was replaced with medium containing 1% FBS. The cell surface (100% confluence) was then scratched using a sterile 200-μl pipette tip and the cells were incubated at 37˚C for 24 h. Each scratch was imaged at 0 and 24 h using an inverted light microscope (Nikon Corporation). The rate of cell migration was measured using ImageJ Plus (version 2.9 011.53t; National Institutes of Health).

Scratch wound healing rate (%)=(initial scratch width-scratch width at observation)/initial scratch width x100.

Transwell assays (6.5 mm Transwell® with 0.4 μm pore polycarbonate membrane insert; cat. no. 3413; Corning, Inc.) were used to measure the longitudinal migration capacity of NSCLC cells treated with different formulations. A total of 2,000 A549 and H460 cells were separately inoculated into Transwell chambers containing medium supplemented with 1% FBS. Complete medium containing 10% FBS was added to the lower chamber. After 24 h incubation at 37˚C, the dead cells were washed and removed from the inside of the Transwell chambers. Subsequently, DAPI staining was performed as aforementioned. The cells were then observed and images were captured using an inverted fluorescence microscope (Motic Incorporation, Ltd.). The number of cells was calculated using ImageJ Plus.

Targeted action of CDDP-PNA-Lip in vivo. In the present study, the construction of a xenograft mouse model was performed by subcutaneous injection. A total of 29 male nude mice (age, 4-6 weeks; weight, 15±2 g) were used in the present study; 9 mice underwent this experiment and 20 mice underwent the subsequent experiment. The mice were maintained in a specific pathogen-free environment at a temperature of 20-26˚C and humidity of 40-70%. The mice were provided free access to sterile food and water and were maintained under a 12-h

light-dark cycle. The humane endpoints were as follows: Tumour volume reaching 10% of body weight of the mouse; the tumour severely affected the mobility or quality of life of the mouse; or if the mouse showed signs of significant pain and distress. Each nude mouse was subcutaneously injected with $5x10^6$ A549 cells diluted with 0.2 ml PBS in the left hind limb. After the tumours were considered palpable, the tumour volume was measured every 2 days. The subcutaneous tumour volume was close to 200 mm^3 when mice with comparable tumour volumes and body weights were selected and randomly divided into three groups [Cy7, Cy7-Lip, Cy7-loaded PNA-modified liposomes (Cy7-PNA-Lip); n=3/group]. Cy7 instead of CDDP was encapsulated into liposomes and the position of Cy7 was reflected by small animal imaging. Cy7-Lip and Cy7-PNA-Lip were prepared to mimic the distribution of CDDP in tumour-bearing nude mice. The mice were injected with 10 mg/kg Cy7, Cy7-Lip or Cy7-PNA-Lip via tail vein within 15 min. Fluorescence images of Cy7 in tumour-bearing nude mice were acquired and analysed using the IVIS Spectrum (PerkinElmer, Inc.) after mice were anaesthetized by inhalation using isoflurane at 2, 4, 8, 12, 24 and 48 h post-injection. During the induction phase, the isoflurane concentration was set at 4%, and during maintenance anaesthesia, the isoflurane concentration was reduced to 2% to maintain stable anaesthesia while reducing the effects on the physiological functions of the mice. The anaesthetic gas was dispersed through oxygen to ensure that the mice received an adequate supply of oxygen throughout the process. All experimental animals were euthanized by CO_2 inhalation 48 h after injection (volumetric emission rate of 4 l/min; ~40% container volume/min) to detect the distribution of Cy7 in major organs and tumour sites in nude mice. Fluorescence images of Cy7 were then acquired and analysed using the IVIS Spectrum Small Animal Live Imaging System and the accompanying software Living Image (version 4.7.2.20319; PerkinElmer, Inc.).

Antitumour efficacy of CDDP-PNA-Lip in vivo. The present study investigated the *in vivo* antitumour activity of CDDP-PNA-Lip by treating nude mice with subcutaneous tumours. An animal model of subcutaneous tumour-bearing nude mice was established using male BALB/C-nu nude mice (age, 4-6 weeks; weight, 15±2 g). The nude mice were housed for 1 week in a specific pathogen-free grade environment at a temperature of 20-26˚C and, humidity of 40-70%. The mice were provided free access to sterile food and water and were maintained under a 12-h light-dark cycle. Each nude mouse was injected subcutaneously with $5x10^6$ A549 cells diluted with 0.2 ml PBS in the left hind limb, and the tumour volume and body weight of the mice were measured every 2 days. A total of 14 days after the subcutaneous injection, the subcutaneous tumour volume in the mice approached 100 mm^3. The mice were then randomly divided into four groups (n=5/group) and administered the following solutions: Saline, CDDP saline solution, CDDP-Lip saline solution or CDDP-PNA-Lip saline solution via intraperitoneal injection. All four solutions were administered at a dose of 2 mg/kg every 4 days for a total of 24 days. Tumour volume and body weight were measured every 2 days. After the length and width of the tumour were measured using digital Vernier callipers, the tumour volume was estimated using the following formula: Tumour volume=(tumour length) x (tumour width)^2 x0.5. Tumour growth inhibition was measured using the following formula: Tumour growth inhibition value (%)=[1-RTV (experimental group)/RTV (control group)] x100, where RTV indicates relative tumour volume.

After 24 days, the animals were euthanized by CO_2 inhalation, blood was collected from the heart, and the tumours, liver, kidney, heart, spleen and lungs were also collected. The tissues were weighed, fixed in 4% paraformaldehyde at room temperature for 6 h and processed. The blood was treated with sodium heparin and centrifuged at 500 x g and 4˚C for 10 min to extract the serum. All organs and tumour tissues were embedded in paraffin for haematoxylin and eosin (H&E) staining. Sections (6 μm) were stained using haematoxylin for 7 min at room temperature and eosin for 1 min at room temperature and were observed under a light microscope, while the serum was analysed for liver and kidney function indicators. Alanine transaminase (ALT; cat. no. H001), alkaline phosphatase (ALP; cat. no. H004), blood urea nitrogen (BUN; cat. no. H044) and creatinine (Cr; cat. no. H047) test kits were obtained from Weifang Kanghua Biotechnology Co., Ltd.

Statistical analysis. The experiments were independently conducted three times. After the data were entered into GraphPad Prism (version 8.0; Dotmatics), statistical analysis was performed using an independent sample t-test for two groups of data or one-way ANOVA followed by Dunnett's multiple comparisons test for three or more groups of data. Data are presented as the mean ± SD. $P<0.05$ was considered to indicate a statistically significant difference.

Results

Bioinformatics analysis of MUC1 in clinical specimens. The bioinformatics analysis of NSCLC tissues revealed that, compared with in normal tissues from patients with lung adenocarcinoma, there was a trend towards elevated expression levels of MUC1 in NSCLC tissues; however, this difference was not significant (Fig. 1B). In addition, >15% of patients with NSCLC exhibited upregulated MUC1 expression (Fig. 1A). These findings suggested that the development of therapeutic regimens targeting MUC1 may be important for patients with NSCLC and has significant clinical implications. Moreover, immunohistochemical staining results from the Human Protein Atlas database revealed that MUC1 was widely and intensively expressed in malignant tumours (Fig. 1C and D), which was consistent with the results of the bioinformatics analysis, further indicating that the present study has good clinical application potential. The results revealed that cells with abnormally elevated tumour MUC1 expression were mainly distributed on the tumour surface, which facilitated the targeting of liposomes for more precise localization at the tumour site.

Synthesis of PNA-modified DSPE. PNA-modified DSPE-PEG2K was synthesized by reacting the active ester (-NHS) of DSPE-PEG2K-NHS with an amino group (-NH_2) on PNA to form an amide bond (-CO-NH-). The successful synthesis of DSPE-PEG2K-PNA was verified by the characteristic peaks of DSPE-PEG2K-PNA detected using infrared spectroscopy and SDS-PAGE (Fig. 2A and B). Images of PEG distribution using PEG dye (Fig. 2Ba) and Coomassie brilliant blue staining of SDS-PAGE gels (Fig. 2Bb) are shown.

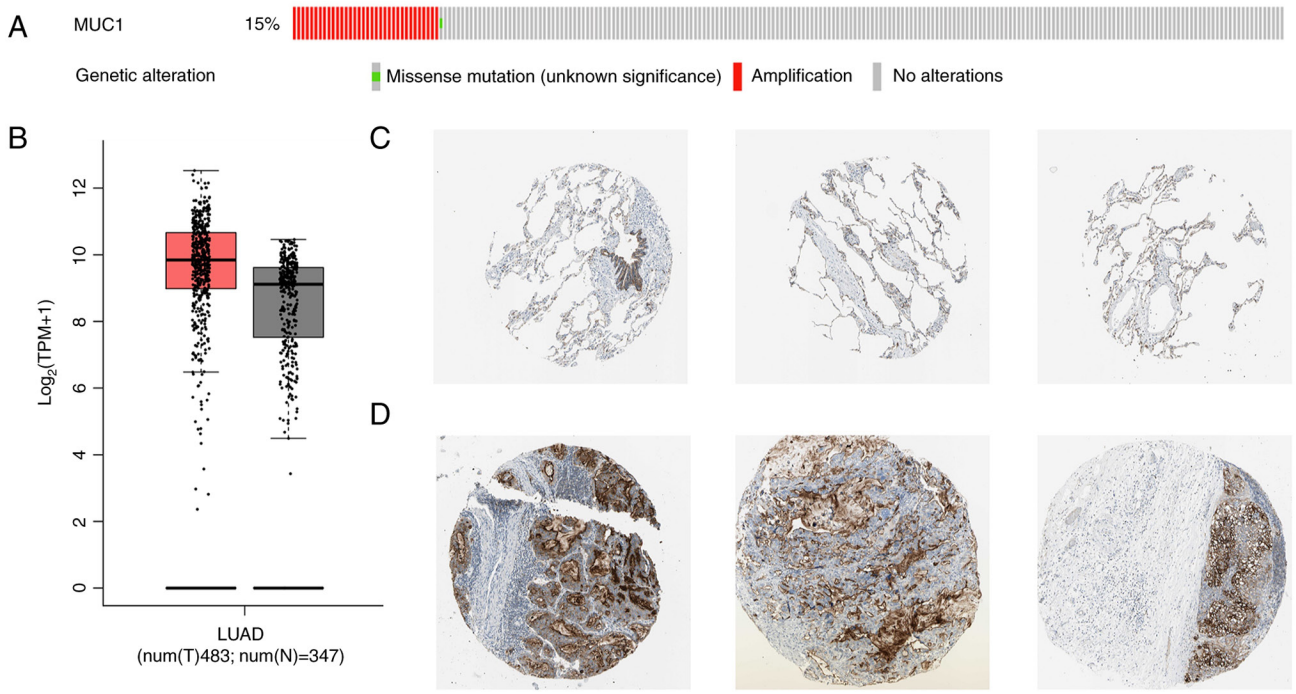

Figure 1. Bioinformatics analysis reveals a trend of high MUC1 expression in patients with non-small cell lung cancer. (A) Proportion of MUC1 gene alterations in patients with lung cancer. The figure was generated by cbioportal (cbioportal.org). (B) MUC1 mRNA expression level in lung cancer tissues were higher than those in paired normal tissues. The figure was generated by GEPIA (gepia.cancer-pku.cn). (C) IHC staining for MUC1 was performed in normal tissues. (D) IHC staining for MUC1 was performed in lung cancer tissues. IHC, immunohistochemical; LUAD, lung adenocarcinoma.

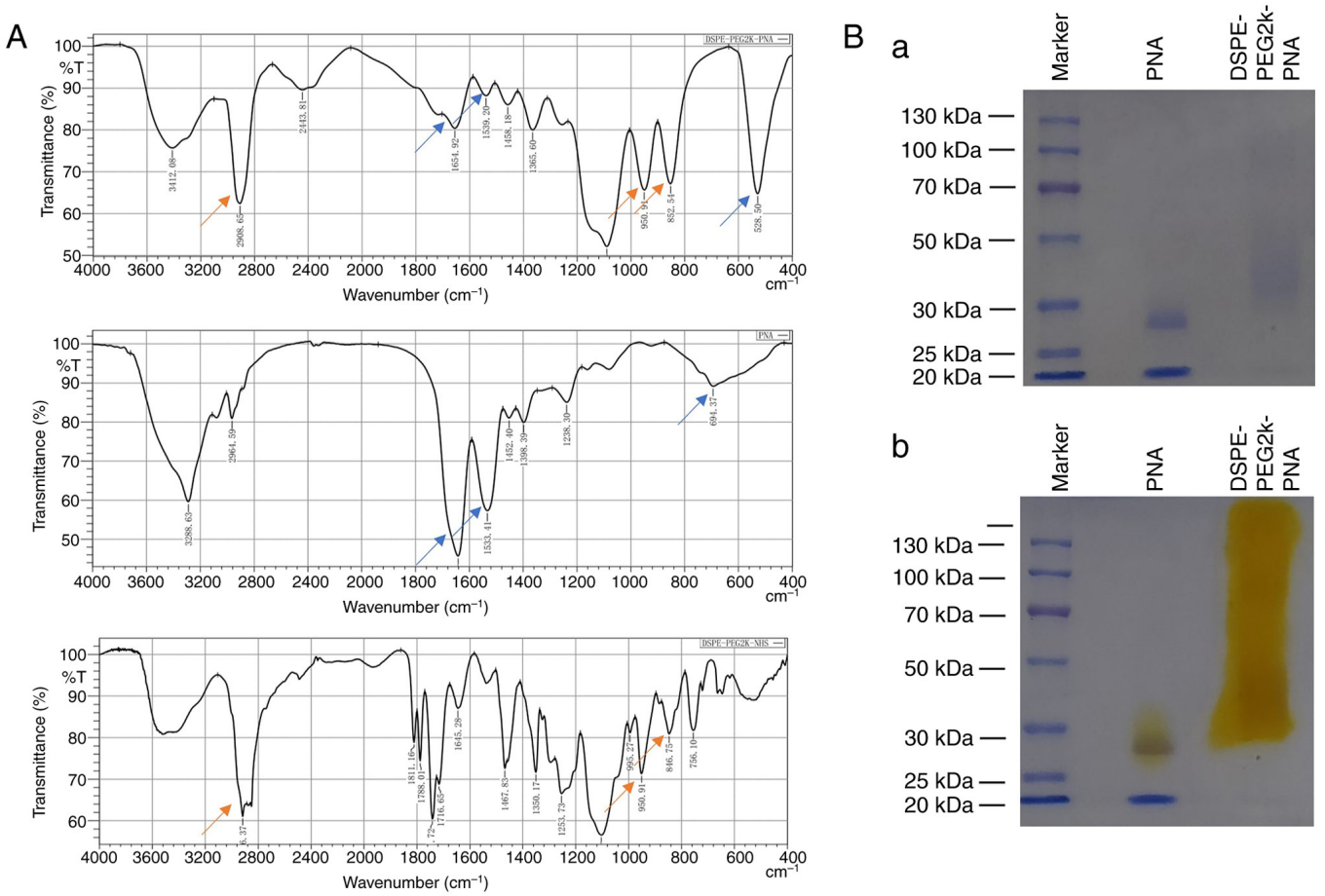

Figure 2. Successful synthesis of DSPE-PEG2K-PNA for subsequent experimental studies. (A) Infrared spectroscopy was used to confirm that the synthesis of DSPE-PEG2K-PNA was successful. (B) SDS-PAGE was used to confirm that PNA was successfully ligated to DSPE-PEG2K. (Ba) Labeling the distribution of proteins using Coomassie brilliant blue staining; (Bb) labeling the distribution of PEG using PEG dye. PNA, peanut agglutinin.

Table I. Characterization of different types of liposomes.

Liposome type	Size, nm	PdI	ζ, mV	EE, %	DL, %
Lip	81.4±0.77	0.258±0.01	-33.7±1.15	-	-
PNA-Lip	83.5±1.92	0.227±0.01	-30.1±1.19	-	-
CDDP-Lip	114.1±3.04	0.214±0.02	-31.4±0.72	35.4±0.24	3.13±0.02
CDDP-PNA-Lip	114.2±1.03	0.203±0.03	-30.7±0.74	35.9±0.14	2.91±0.01

Data are presented as the mean ± SD (n=3). CDDP, cisplatin; DL, drug loading; EE, entrapment efficiency; PdI, polydispersity index; PNA, peanut agglutinin; PNA-Lip, PNA-modified liposomes; CDDP-Lip, CDDP-loaded liposomes; CDDP-PNA-Lip, CDDP-loaded PNA-modified liposomes.

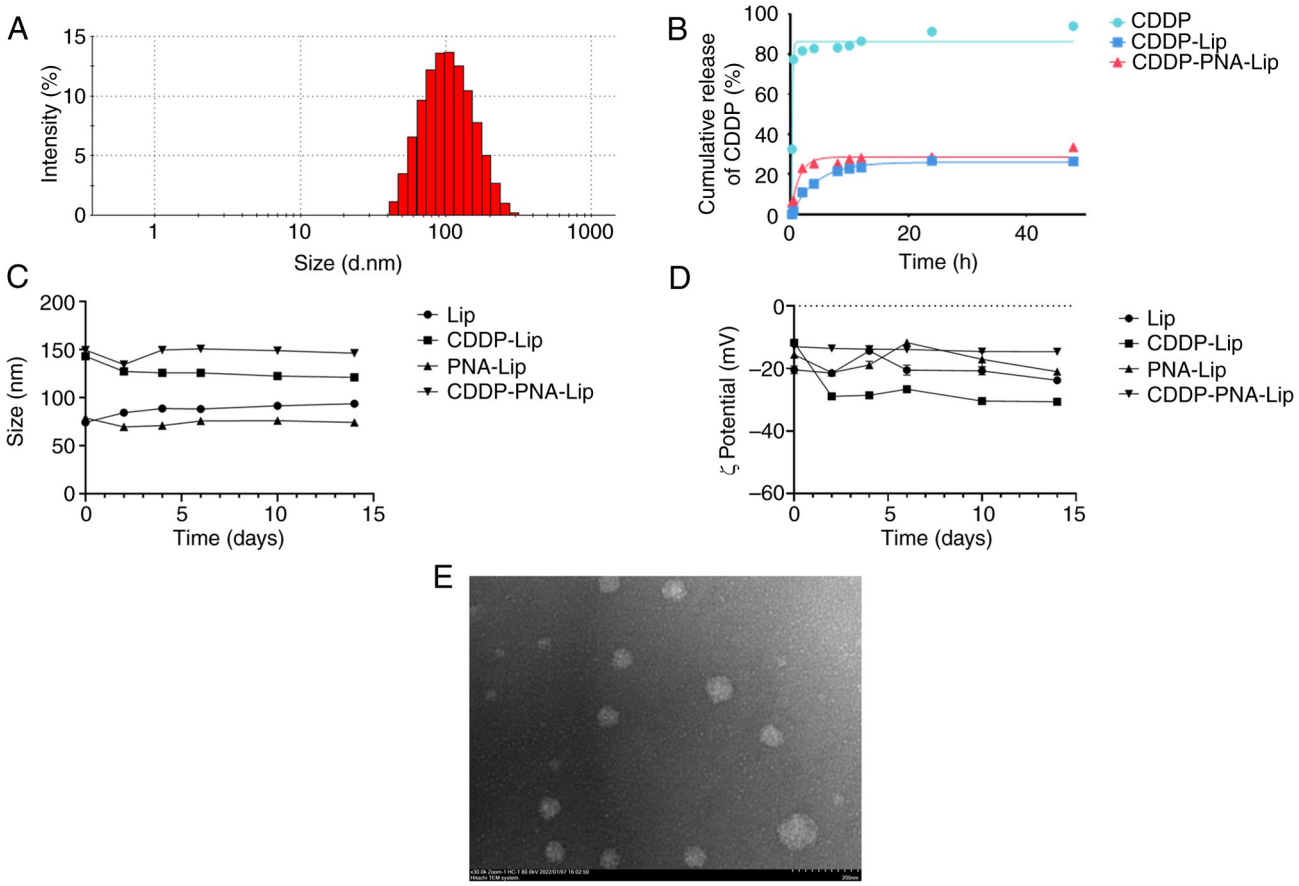

Figure 3. Preparation of liposomes with good stability and drug release effect. (A) Particle size distribution of CDDP-PNA-Lip. (B) Cumulative drug release profiles of CDDP-Lip in PBS at 37˚C for 48 h. (C) Potential changes in the particle size of different types of liposomes stored in saline at 4˚C for 14 days. (D) Potential changes in the ζ potential of different types of liposomes stored in saline at 4˚C for 14 days. (E) Projection electron microscopic images (magnification, x30,000). CDDP, cisplatin; PNA, peanut agglutinin; Lip, blank liposomes; PNA-Lip, blank PNA-modified liposomes; CDDP-Lip, CDDP-loaded liposomes; CDDP-PNA-Lip, CDDP-loaded PNA-modified liposomes.

Preparation of stable liposomes and CDDP-Lip. As shown in Table I and Fig. 3A, the prepared CDDP-PNA-Lip were heterogeneous and stable, and could effectively encapsulate CDDP. The particle sizes of Lip and PNA-Lip were ~80 nm, while the particle size of the liposomes increased to ~120 nm after encapsulating CDDP. This increase in size is likely due to the electrostatic force of some of the CDDP molecules on the surface of the liposomes. The polydispersity index of each liposome was ~0.2, which represented good lipid homogeneity. The ζ potential of CDDP-Lip was ~-30 mV, and the encapsulation of CDDP did not result in a change in the surface charge. This finding is consistent with the findings of other protocols for DL that rely on electrostatic forces of adsorption (24). The EE was >35%, and the DL capacity was greater than 3%. This DL capacity was greater than that of reported CDDP-Lip (32), which achieved only a 1% DL capacity. Since the DL of CDDP was achieved through electrostatic adsorption of liposomes, it led to an increase in the particle size of liposomes encapsulating CDDP compared to those that were not encapsulated. The morphology of the CDDP-PNA-Lip was observed using a TEM. The results indicated that the PNA-CDDP-Lip were uniform three-dimensional spheres with smooth surfaces and particle sizes (Fig. 3E).

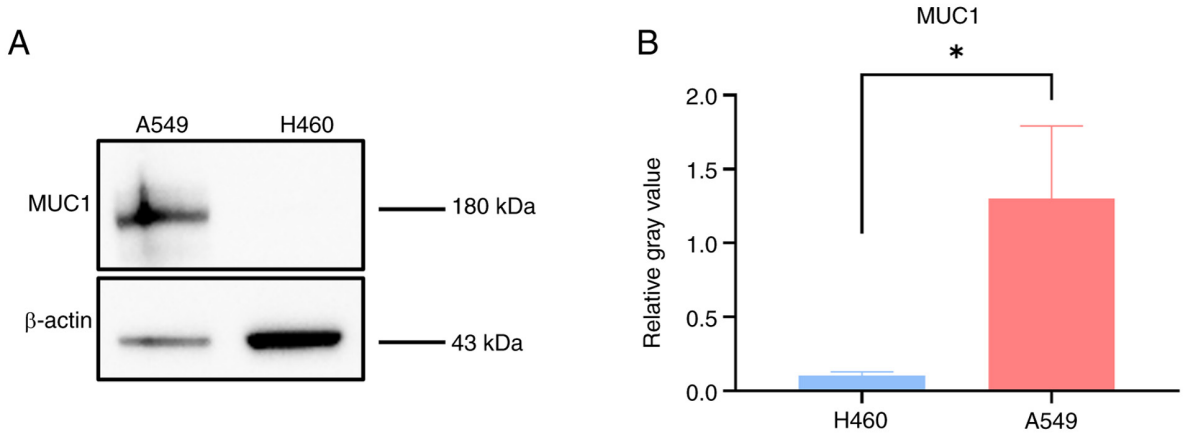

Figure 4. Determination of MUC1 expression in non-small cell lung cancer cell lines. (A) Western blot analysis of MUC1 expression in two cell lines. (B) Semi-quantitative analysis of the western blotting results. *P<0.05.

The *in vitro* dialysis experiments were performed using dialysis bags, and the *in vitro* release profile of CDDP-Lip is shown in Fig. 3B. Depending on the release rate, the cumulative release of CDDP from unmodified liposomes exhibited two distinct phases, i.e., a rapid release phase and a sustained release phase. The rapid release phase lasted for ~2 h, during which ~20% of the CDDP was released from the liposomes; this phase was followed by a sustained release phase, during which CDDP continued to be slowly released; the cumulative release of the drug was ~35% after 48 h of the experiment. Although the cumulative release of CDDP from the modified liposomes also showed two phases, its release profile was smoother than that of unmodified liposomes, and it had a better slow-release effect than that of unmodified liposomes within 12 h. Notably, ~20% of CDDP was released from CDDP-PNA-Lip in the first 4 h, followed by a sustained release phase at a slower rate; the first 20% seemed to be more quickly released from CDDP-PNA-Lip than from CDDP-Lip within 4 h. It was hypothesized that this result may be due to the addition of phospholipids containing PEG components within the liposomes, which allowed CDDP-Lip and CDDP-PNA-Lip to exhibit a sustained and stable release during the experiment. The results suggested that encapsulating CDDP with liposomes may prolong the release time of the drug, which is beneficial for achieving sustained release at the tumour target (Fig. 3B).

All the liposomes were diluted 10-fold with ddH_2O and stored at 4˚C in the dark. The particle size and potential of the liposomes were monitored every 2 days, and the corresponding change curves are presented in Fig. 3C and D. The particle size of all the liposomes fluctuated within a range of ±10 nm and did not change significantly across 15 days. Similarly, the potential did not vary significantly, indicating that the liposomes prepared in the present study were stable.

Determination of MUC1 expression in cells. Western blotting was used to detect the expression levels of MUC1 in the A549 and H460 cell lines. The grayscale analysis revealed that MUC1 was expressed at significantly higher levels in A549 cells than in H460 cells (Fig. 4A and B).

PNA-Lip enhance the delivery efficiency to MUC1-positive NSCLC cells. The effect of ligand modification on improving the liposomal delivery efficiency was explored by performing *in vitro* cellular uptake assays (Fig. 5). The MUC1-negative NSCLC cell line used in the experiment was H460, and the MUC1-positive NSCLC cell line was A549. The impact of the ligand modification on enhancing the efficiency of liposomal drug delivery was studied by examining the cellular uptake of each liposome type using confocal laser scanning microscopy (CLSM). The uptake of each type of RhB liposome was assessed in A549 and H460 cells after 6 h. As shown in Fig. 5A and B, CLSM revealed the strongest red fluorescence in the A549 cell line treated with RhB-PNA-Lip. The quantitative analysis showed that the intensities of red fluorescence in the RhB-PNA-Lip group were 1.53 and 1.24-fold greater than those in the RhB and RhB-Lip groups, respectively. These results indicated that the PNA modification enhanced the uptake of liposomes by A549 cells. By contrast, RhB-PNA-Lip did not exhibit a stronger fluorescence intensity in the H460 cell line. These findings suggested that the modification of liposomes with PNA significantly improved their targeting effect on MUC1-positive NSCLC cells, such as A549 cells.

PNA-Lip exhibit enhanced antitumour efficacy in MUC1-positive NSCLC cells in vitro. Investigations into the cytotoxic efficiency of ligand-modified liposomes were conducted using the MTS assay to determine the viability of A549 and H460 cells treated with CDDP-Lip. The MTS assay results showed no significant difference in cytotoxicity between CDDP and hydrated CDDP in the two cell lines (Fig. 6A and B), which was previously described by Lippard (31), where hydrated CDDP regenerated CDDP in the presence of Cl^-, which did not affect its antitumour activity. After treating A549 and H460 cells with CDDP, CDDP-Lip and CDDP-PNA-Lip for different durations, it was revealed that CDDP had a dose-dependent antitumour effect. After 48 h of drug treatment, the A549 cells in the CDDP-PNA-Lip treatment group exhibited the lowest cellular viability, which was not observed in the three treatment groups of H460 cells (Fig. 6C-F). This finding suggested that the ligand-modified liposomes may have greater delivery efficiency and stronger cytotoxicity against MUC1-positive NSCLC cell lines.

The results of the MTS experiments prompted the evaluation of the apoptosis of A549 and H460 cells treated for 48 h with

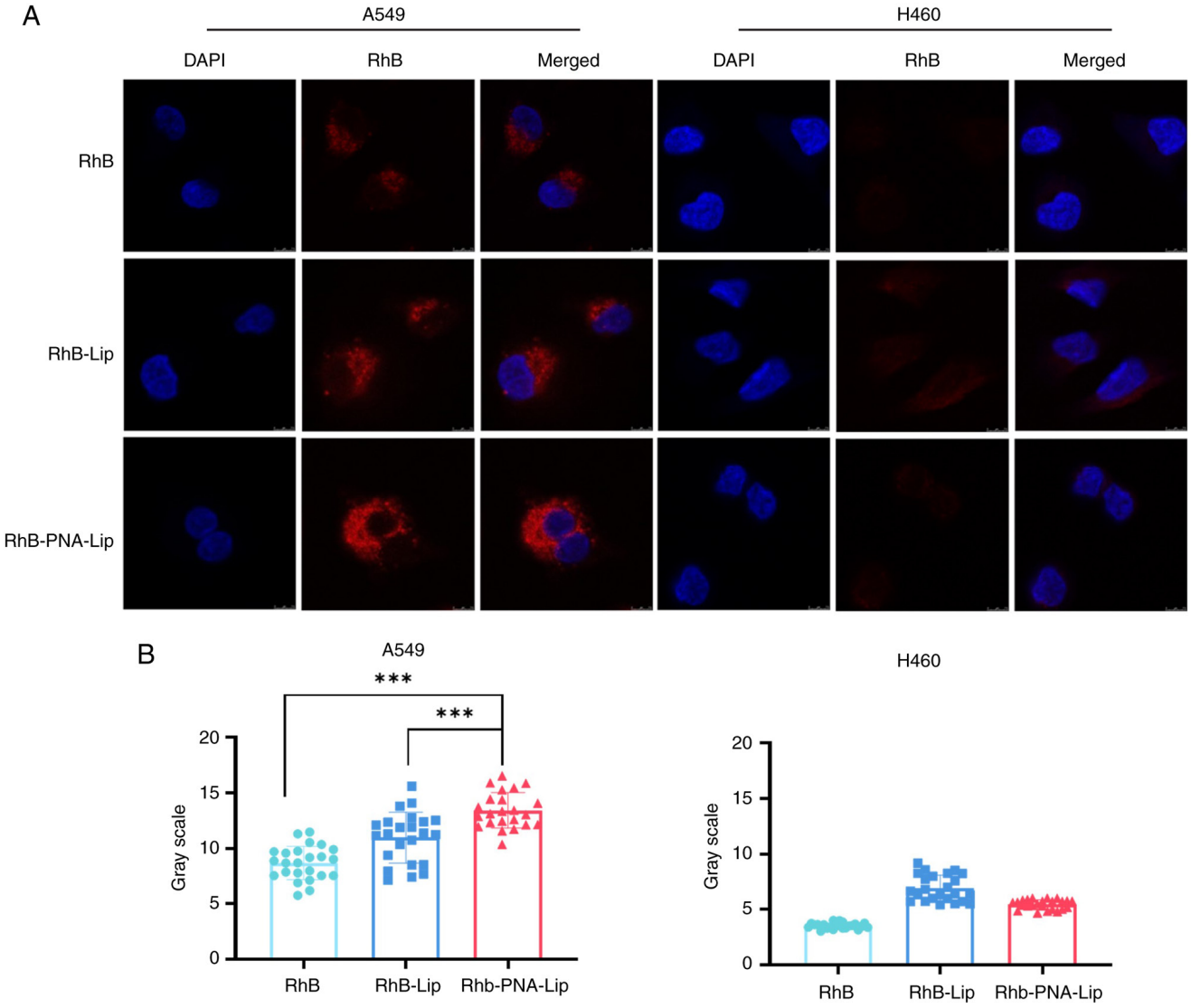

Figure 5. PNA-modified liposomes enhance the delivery efficiency to MUC1-positive non-small lung cancer cells. (A) Confocal laser scanning microscopy observation of the distribution of fluorescent signals in A549 and H460 cells (magnification, x60). (B) Quantitative analysis of RhB fluorescent signals in A549 and H460 cells. ***P<0.001. RhB, Rhodamine B; PNA, peanut agglutinin; RhB-Lip, RhB-loaded liposomes; RhB-PNA-Lip, RhB-loaded PNA-modified liposomes.

2.5 μg/ml CDDP and liposomes. The levels of Annexin V on the cell surface were detected using flow cytometry. The results revealed no significant difference in the effects of CDDP-Lip or CDDP-PNA-Lip on early apoptosis in MUC1-negative H460 cells (Fig. 6G). For MUC1-positive A549 cells, the percentage of apoptotic cells in the CDDP-PNA-Lip group was 1.5 times higher than that in the CDDP-Lip group (Fig. 6G). These findings suggested that modification of CDDP-Lip with PNA may induce the apoptosis of MUC1-positive NSCLC cells.

Notably, the utilization of liposomes to encapsulate CDDP seems to diminish its antitumour efficacy on H460 cells. It may be hypothesized that this is because liposomes exhibit a sustained-release effect on the drug, and cells uptake liposomes with varying efficiency. This phenomenon was also observed by Diao *et al* (33).

PNA-Lip enhance the antimigratory efficacy of MUC1-positive NSCLC cells in vitro. Cell scratch wound assays and Transwell assays were used to verify the lateral and longitudinal migration abilities of the different PNA-modified liposomes. For the cell scratch wound assay, normal saline, free CDDP, CDDP-Lip or CDDP-PNA-Lip were added to the scratched cells in 6-well plates, which were subsequently cocultured with the cells for 24 h. Images of the cells were captured at 0 and 24 h. The scratch wound healing rate of the A549 cells in the normal saline group was 19.32±2.93%, whereas that in the CDDP-PNA-Lip group was the smallest, with a scratch wound healing rate of 9.08±2.03% (Fig. 7A and C). These rates were significantly lower than those in the CDDP group and CDDP-Lip group (14.38±1.48 and 14.59±2.51%, respectively). The healing rate of the saline group (13.77±1.89%) was notably higher than that of the free CDDP, CDDP-Lip and CDDP-PNA-Lip groups (8.36±2.81, 8.26±2.83 and 9.00±2.58%, respectively) in A549 cells; however, no significant differences were observed among the drug treatment groups in H460 cells (Fig. 7A and C).

In the Transwell assay, the cells were cultured for 24 h, stained with DAPI and images were captured using an inverted fluorescence microscope. The number of A549 cells

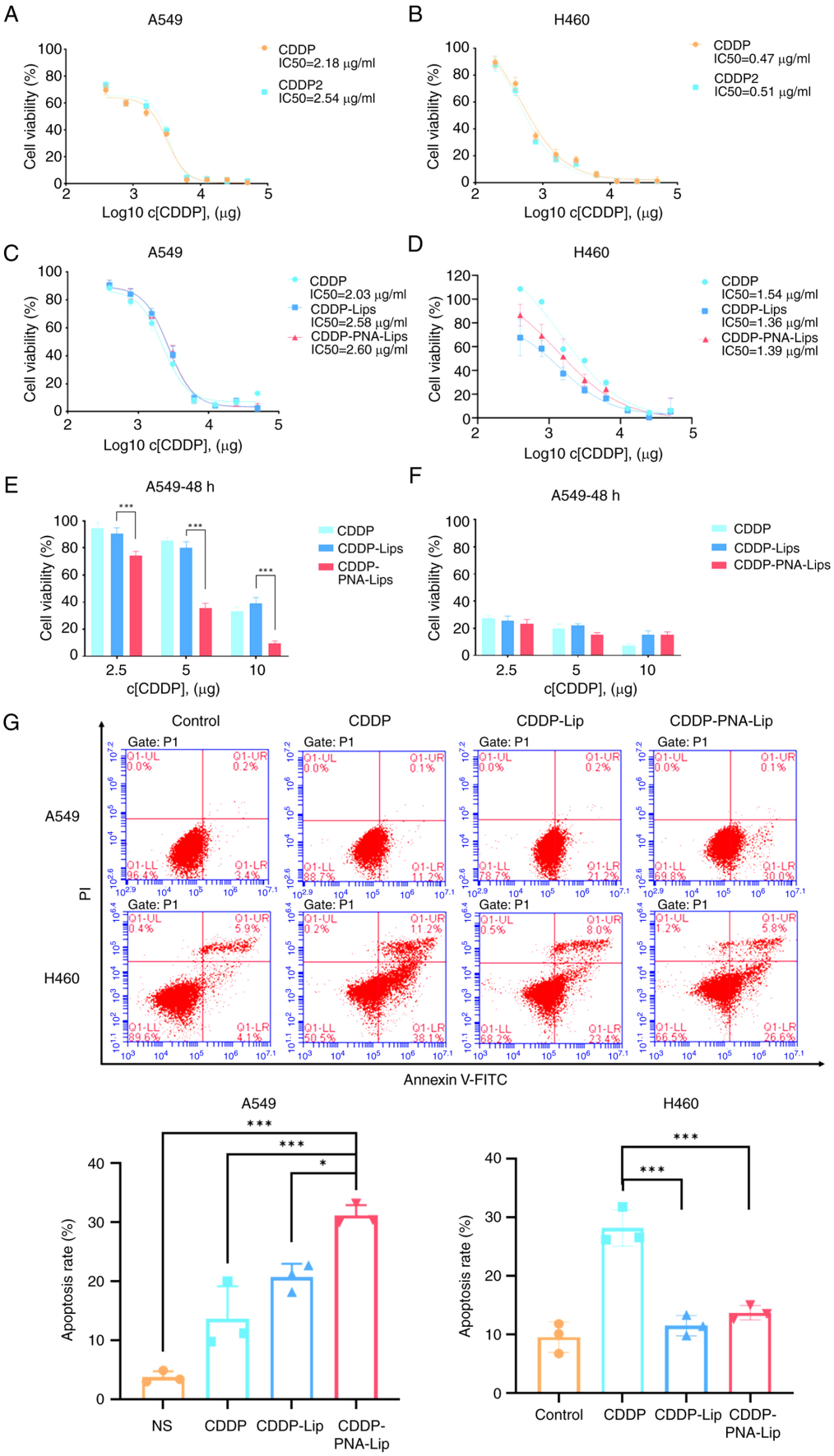

Figure 6. PNA-modified liposomes have good antitumour effects and induce the apoptosis of MUC1-positive NSCLC cells *in vitro*. Comparison of antitumour activity against (A) A549 and (B) H460 cells before and after drug modification. CDDP is hydrated cisplatin, CDDP2 is untreated cisplatin. IC50 values of CDDP and drug-loaded liposomes in (C) A549 and (D) H460 cells after treatment duration for 72 h. Effects on the viability of (E) A549 and (F) H460 cells after treatment with 2.5, 5 and 10 μg/ml CDDP and drug-loaded liposomes for 48 h. (G) Effect of drug-loaded liposomes on apoptosis. *P<0.05, ***P<0.001. CDDP, cisplatin; PNA, peanut agglutinin; CDDP-Lip, CDDP-loaded liposomes; CDDP-PNA-Lip, CDDP-loaded PNA-modified liposomes.

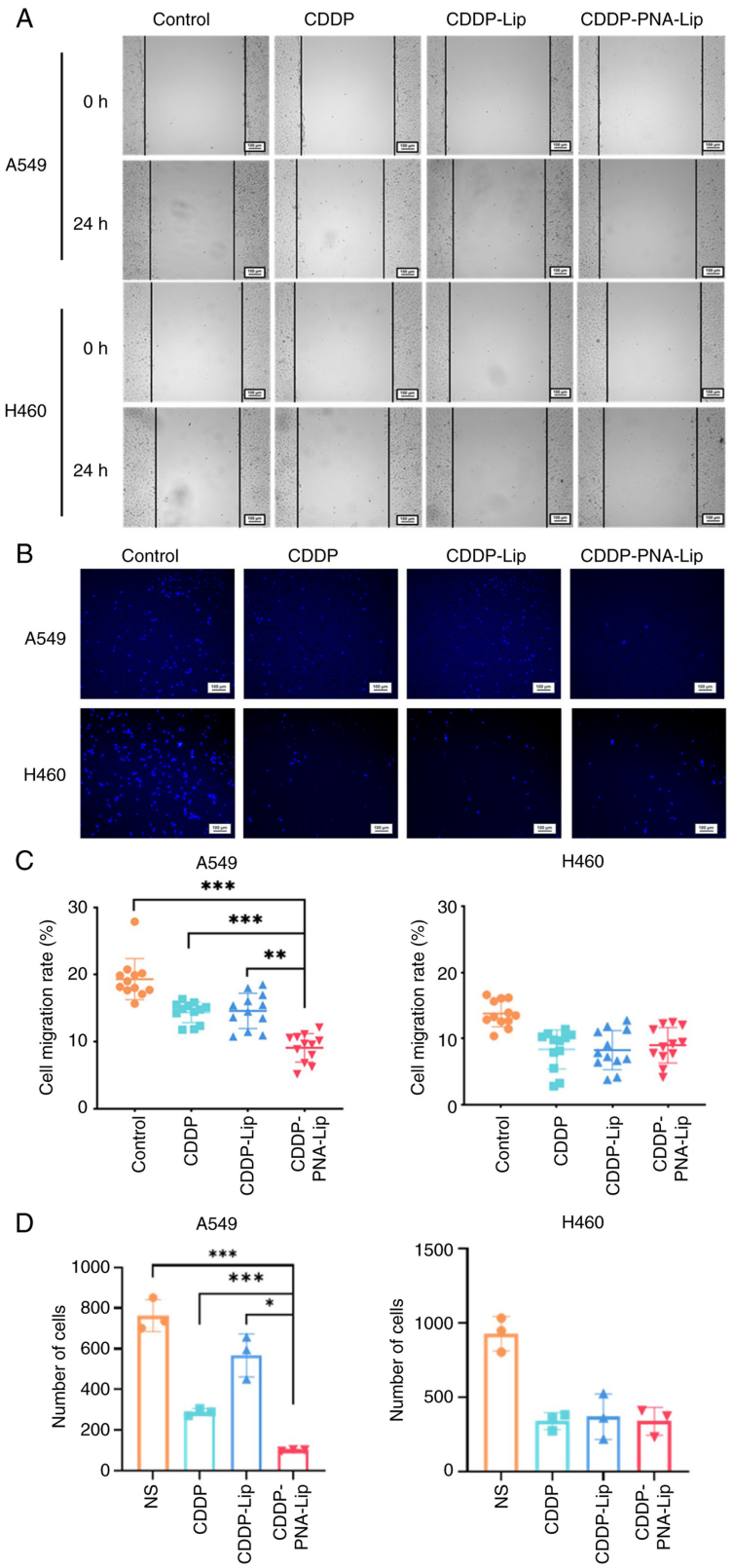

Figure 7. Cell scratch wound and Transwell assays show that PNA-modified liposomes inhibit the migration of MUC1-positive non-small cell lung cancer cells. (A) Cell scratch wound assay of two cell lines treated with different types of liposomes (magnification, x10). (B) Transwell assay of two cell lines treated with different types of liposomes (magnification, x20). (C) Quantitative analysis of the cell scratch wound assay. (D) Quantitative analysis of the Transwell assay. *P<0.05, **P<0.01, ***P<0.001 CDDP, cisplatin; PNA, peanut agglutinin; CDDP-Lip, CDDP-loaded liposomes; CDDP-PNA-Lip, CDDP-loaded PNA-modified liposomes.

treated with CDDP-PNA-Lip was the lowest in the field of view and was significantly lower than that in the other groups; however, no significant differences were observed in H460 cells (Fig. 7B and D). These results indicated that the ability of liposomes to inhibit tumour cell migration was enhanced when they were modified with PNA.

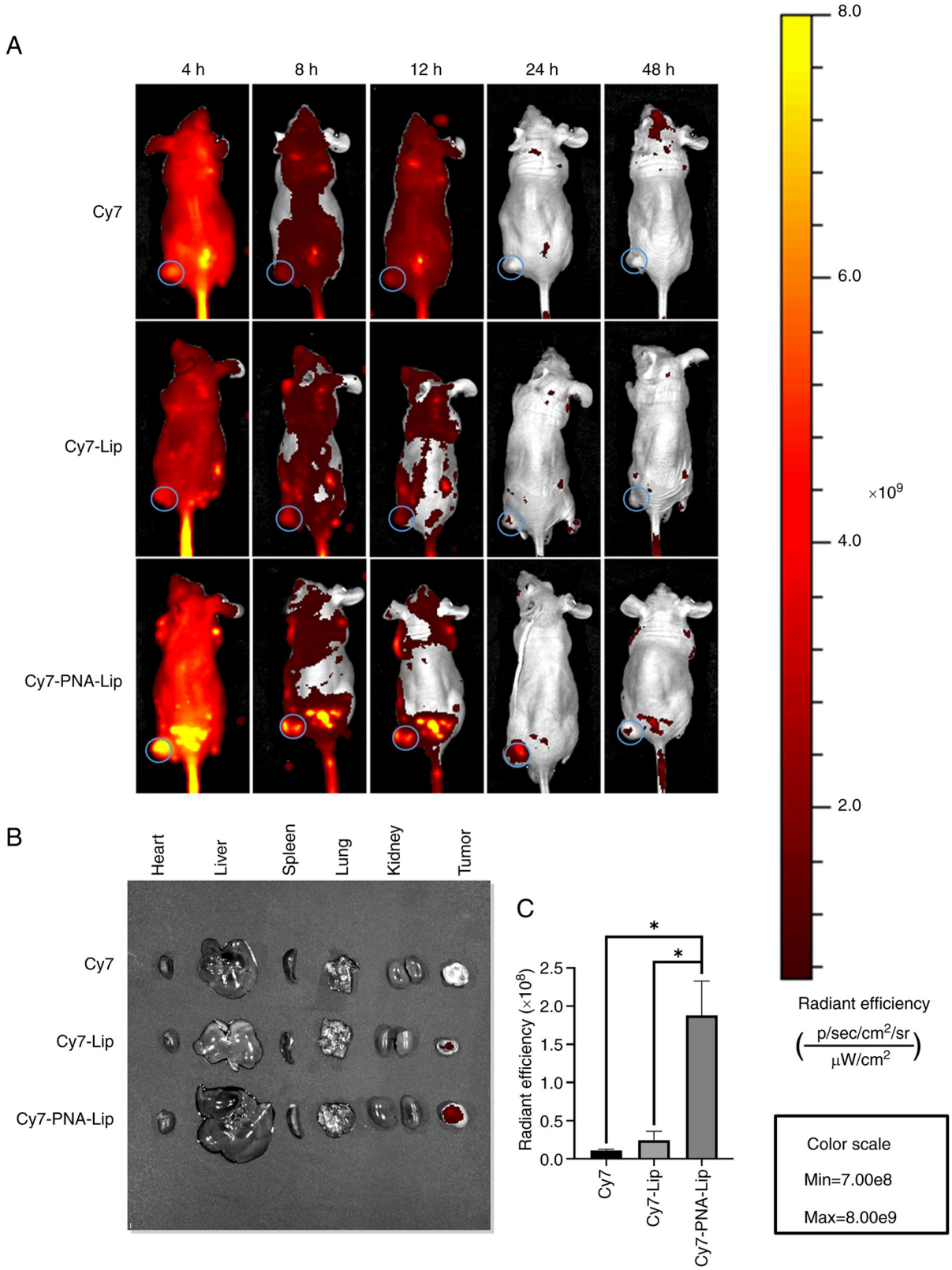

Figure 8. A xenograft mouse model shows that PNA-modified liposomes enhance tumour-targeting efficacy *in vivo*. (A) Distribution of Cy7 in tumour-bearing nude mice after a tail vein injection. (B) Distribution of Cy7 in vital organs and tumour tissues after 48 h. (C) Quantitative analysis of fluorescent signals in tumours. *P<0.05. Cy7, sulfo-Cyanine7 carboxylic acid; PNA, peanut agglutinin; Cy7-Lip, Cy7-loaded liposomes; Cy7-PNA-Lip, Cy7-loaded PNA-modified liposomes.

PNA-Lip exhibit enhanced tumour targeting in a xenograft mouse model. The effects of the ligand modification on enhancing target acquisition *in vivo* were investigated by monitoring animals with near-infrared fluorophore imaging. Cy7 was encapsulated in liposomes to mimic the circulation of CDDP in nude mice. Cy7, Cy7-Lip and Cy7-PNA-Lip were

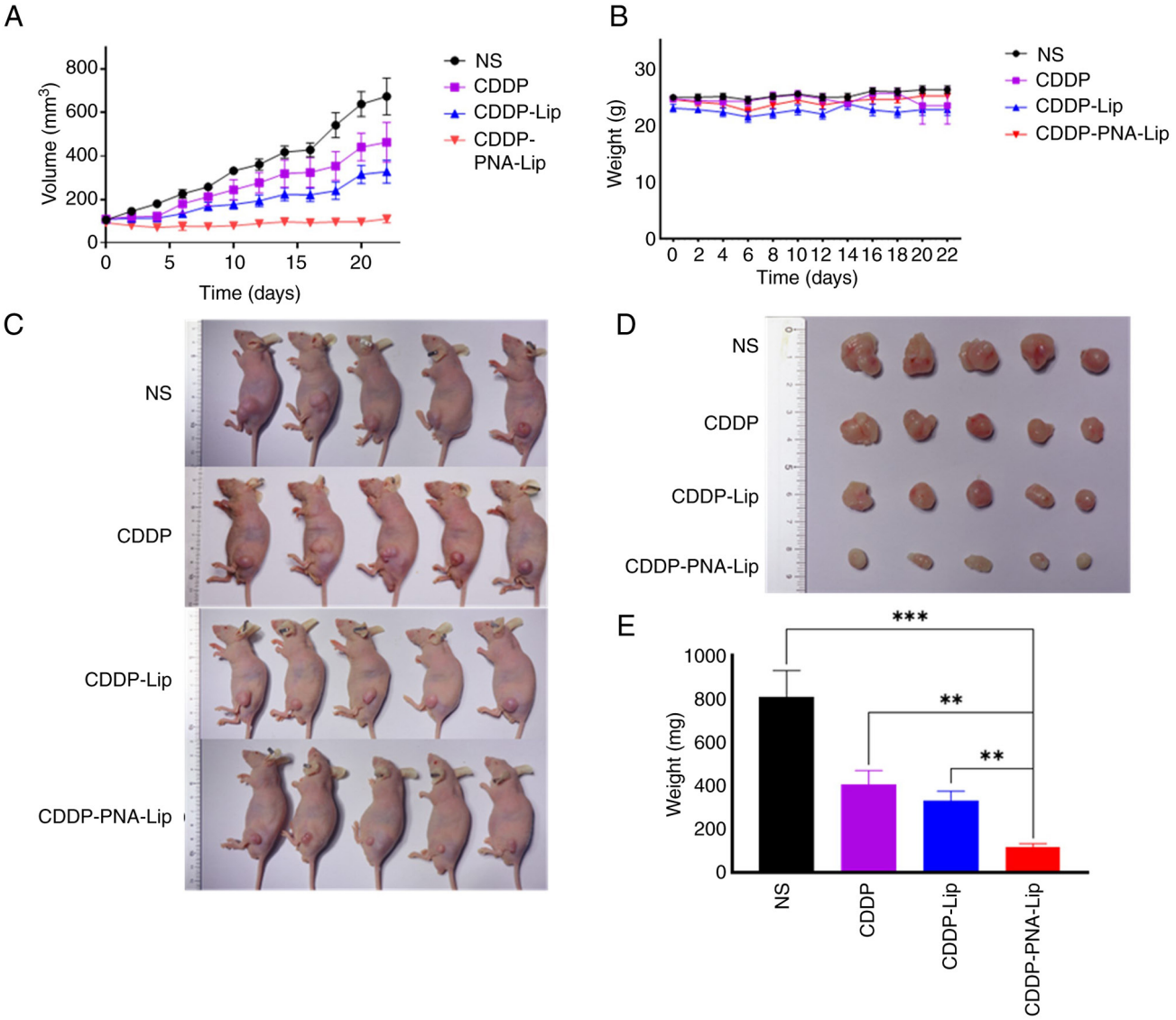

Figure 9. A xenograft mouse model shows that PNA-modified liposomes significantly enhance the antitumour efficacy *in vivo*. Changes in the (A) tumour volumes and (B) body weights of the tumour-bearing nude mice. (C) Images of tumour-bearing nude mice in each group after 24 days of treatment. (D) Images of the tumours of tumour-bearing nude mice after they were collected (E) Histograms of tumour weights. **P<0.01, ***P<0.001. CDDP, cisplatin; PNA, peanut agglutinin; CDDP-Lip, CDDP-loaded liposomes; CDDP-PNA-Lip, CDDP-loaded PNA-modified liposomes.

then injected into the nude mice via the tail vein. A total of 4 h after injection, Cy7-PNA-Lip began to distribute predominantly to the tumour site in nude mice and was most evident at 8 h. Over time, Cy7 was metabolized and excreted from the nude mice. The fluorescent signal in the bodies of the mice gradually weakened, and all residual fluorescence disappeared completely after 24 h (Fig. 8A). Observations of mice injected with Cy7-PNA-Lip revealed that the fluorescent signal at the tumour site was markedly stronger than that in mice injected with Cy7 or Cy7-Lip. This high signal intensity persisted for 48 h. Before the nude mice were euthanized, the mice injected with Cy7-PNA-Lip still exhibited notably greater fluorescent signals at the tumour site than the other two groups (Fig. 8A). Subsequently, the mice were euthanized, fluorescence imaging was conducted, and an analysis of their major organs and tumour sites was performed. The results revealed that the tumours of nude mice injected with Cy7-PNA-Lip still exhibited strong fluorescent signals even after 48 h (Fig. 8B and C). Furthermore, due to the absence of an epidermal barrier, the fluorescence intensity at the tumour sites was significantly higher in the Cy7-PNA-Lip-injected nude mice than in the other two groups. These results indicated that the *in vivo* targeting ability of PNA-Lip aligns with the results of cellular uptake. Furthermore, the PNA modification of liposomes may enable them to actively target tumours. In addition, based on the change in the fluorescence intensity of Cy7 within the tumours of Balb/c-nu mice, the modification of liposomes with PNA extends the duration of drug presence in tumours and enhances drug accumulation at the tumour site. It was thus hypothesized that the utilization of PEG and PNA may enhance the active targeting ability of a drug and prolong its presence at the tumour site. These characteristics, in turn, could reduce the required drug dosage and frequency of administration.

PNA-Lip exhibit enhanced antitumour efficacy in a xenograft mouse model. The *in vivo* antitumour efficacy of

CDDP-PNA-Lip was evaluated by treating nude mice bearing subcutaneous tumours with saline, CDDP, CDDP-Lip or CDDP-PNA-Lip. By monitoring and analysing the body weights of the animals, no significant weight loss was observed in any of the four groups after drug administration (Fig. 9B). This finding suggested that the drug treatment had few toxic side effects. After the initial treatment (day 0; Fig. 9A), the growth of the tumour tissue stopped in all groups of subcutaneous tumour-bearing nude mice. However, as the number of doses increased (from day 4; Fig. 9A), the tumour tissue in the subcutaneous tumour-bearing nude mice treated with CDDP and CDDP-Lip continued to grow, whereas that in the mice treated with CDDP-PNA-Lip showed sustained tumour suppression. The results indicated that CDDP-PNA-Lip exerted the strongest antitumour effect, with a tumour inhibition rate of 83.1%. The tumour volume of the mice treated with CDDP was 2.65 times larger than that of the mice treated with CDDP-PNA-Lip, while the tumour volume of the mice treated with CDDP-Lip was 1.63 times larger than that of the mice treated with CDDP-PNA-Lip. At the end of the treatment, all mice were sacrificed and the tumours were weighed, the results showed that mice treated with CDDP-PNA-Lip had the smallest tumour weights, which were significantly different compared with the other groups (Fig. 9C-E). H&E staining revealed that the tumour tissues in the saline control group were densely packed, whereas those in the CDDP-PNA-Lip group exhibited the highest levels of apoptosis and necrosis. A large number of vacuoles appeared between the tissues, indicating the significant antitumour efficacy of CDDP-PNA-Lip (Fig. 10A). The modification of liposomes with PNA significantly enhanced the antitumour efficacy of the liposomes against NSCLC tissues with high MUC1 expression.

PNA-Lip improve the toxicity and side effects of CDDP in vivo. The biosafety and antitumour effects of CDDP-PNA-Lip were evaluated using H&E staining. After histological sectioning and staining of the heart, liver, spleen, lungs and kidneys, no histopathological abnormalities were found in any of the four groups of animals (Fig. 10A). The effect of CDDP-PNA-Lip on liver and kidney function in nude mice was evaluated by measuring physiological indicators of liver and kidney function in serum (Fig. 10B). The results showed that biochemical indices, such as Cr, ALT, ALP and BUN, were not significantly altered in any of the groups. These results indicated that liposomes modified with PNA and containing CDDP colloids do not cause significant systemic toxicity in experimental mice.

Discussion

Lung cancer ranks second in global cancer incidence and first in mortality, and is therefore considered one of the greatest threats to human health (34). In addition, primary treatments for lung cancer, such as surgery, radiotherapy or chemotherapy, carry a significant risk of recurrence. Based on the histopathological classification, lung cancer can be divided into two groups: Small cell lung cancer and NSCLC (34,35). Among lung cancer types, NSCLC has a high incidence rate, accounting for 80-85% of all lung cancer cases, and is particularly difficult to cure (36). Among the therapeutic options for NSCLC, CDDP, a broad-spectrum anticancer drug, has shown efficacy as a first-line treatment for lung cancer (37,38). However, due to the evident nephrotoxicity of CDDP, its clinical application has been somewhat restricted (7). It has been shown that the use of liposome-encapsulated drugs not only decreases their toxic side effects but also extends the duration of drug circulation in the body. Due to the ease of modifying the liposome surface, the binding of ligands to the liposome surface can enable the liposome to acquire an active targeting ability. This property, in turn, reduces nonspecific drug release from liposomes (39).

Based on previous research, it was hypothesized that using liposomes to encapsulate CDDP and modification of their surface is a feasible option for NSCLC treatment. Modification of liposomes with PNA enables specific active targeting of tumour tissues in NSCLC with high expression of MUC1 (23,33). The surface of MUC1 expressed in normal tissues is highly glycosylated due to the properties of MUC1, which makes it untargeted. As observed in the present animal experiments, fluorescence did not accumulate outside the tumour site in the Cy7-PNA-Lip group, and no marked damage was observed in the major organs of the animals in the CDDP-PNA-Lip group. This finding suggested that targeted therapy against tumour MUC1 may have promising applications. Notably, in a study by Lozano *et al* (40), the utilization of the MUC1 monoclonal antibody hCTM01 to modify PGE-conjugated liposomes for the smooth encapsulation of antitumour drugs resulted in marked antitumour effects both *in vivo* and *ex vivo*. Furthermore, the efficacy of antitumour therapy can be enhanced by combining the targeting of MUC1 with other targeting sites. This combination was reported in a study by Kim *et al* (41), where co-targeting of CD44 and MUC1 was achieved through dual aptamer modification of liposomes, leading to targeted killing effects on tumour stem cells and tumour cells. In addition, targeting MUC1 via antibody-drug conjugates (ADCs) has been suggested as another effective method of antibody therapy. In a study by Panchamoorthy *et al* (42), a monomethyl auristatin E-conjugated MUC1-C monoclonal antibody ADC was constructed and was shown to achieve targeted killing of MUC1-C-overexpressing tumours *in vitro* and *in vivo*. Ranjbar-Navazi *et al* (43) constructed a nanosystem consisting of a MUC1 aptamer and nanohydrogels and quantum dots, and achieved effective loading of paclitaxel and sodium oxalate. In *in vitro* studies, this nanosystem was able to target MCF-7 breast cancer cells and significantly induced mitochondria-mediated apoptosis.

For liposomal encapsulation, the solubility of the drug is one of the key factors that affects the encapsulation efficiency. The present study used the hydration reaction of CDDP to pretreat the drug and create a positively charged surface. Moreover, DPPG, a commonly functionalized phospholipid, was added to the liposomes to create a negatively charged surface. Hydrated CDDP can be efficiently carried through electrostatic adsorption. By combining the aforementioned techniques with our research on liposome preparation, the stable encapsulation and targeted delivery of CDDP was successfully achieved. Compared with the DL capacity of SPI-077 (a class of liposomes coated with CDDP), the liposomes created in the present study achieved a significant increase in the DL capacity of CDDP (3%), while also enabling active targeting to tumour sites in animals (11,44).

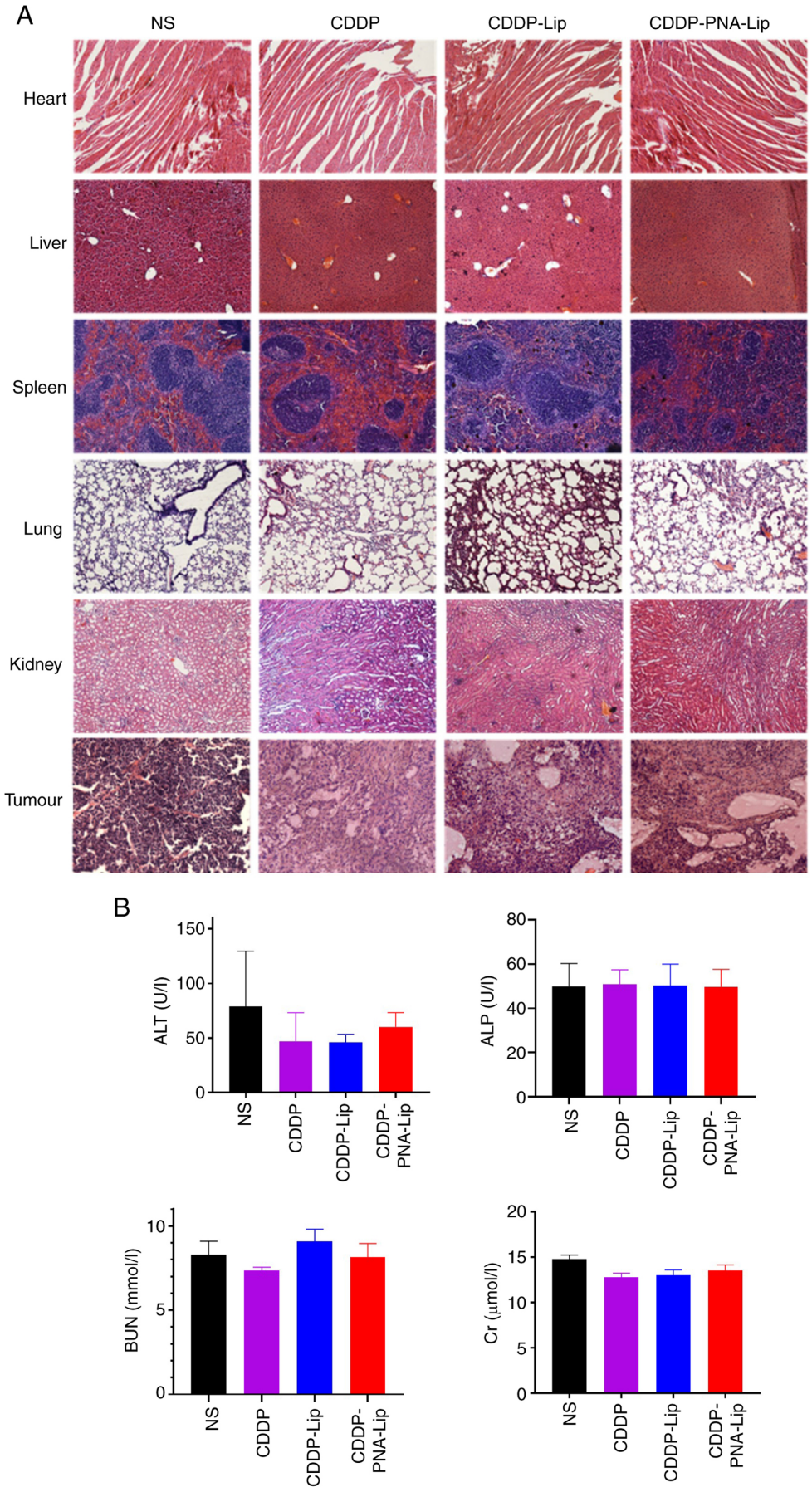

Figure 10. A xenograft mouse model shows that PNA-modified liposomes have no systemic toxicity *in vivo*. (A) Haematoxylin and eosin staining of vital organs and tumours (magnification, x20). (B) Analysis of physiological indices of the liver and kidney. ALP, alkaline phosphatase; ALT, alanine transaminase; BUN, blood urea nitrogen; CDDP, cisplatin; Cr, creatinine; NS, normal saline; PNA, peanut agglutinin; CDDP-Lip, CDDP-loaded liposomes; CDDP-PNA-Lip, CDDP-loaded PNA-modified liposomes.

These results were validated in both *in vivo* and *in vitro* experiments. Although the apoptosis-inducing efficiency of CDDP decreased after encapsulation with PNA-Lip in *in vitro* experimental studies on H460 cells, this phenomenon may be attributed to the variance in cellular uptake of liposomes and CDDP. The cellular uptake of the free drug is primarily influenced by drug concentration; however, in the present *in vivo* experiments, small-animal imaging showed that liposome-encapsulated drugs accumulated more effectively at the tumour site. Consequently, the drug concentration at the tumour site was notably higher than that of the free drug until the drug was fully metabolized, thereby not affecting the application of CDDP. Moreover, the liposomes may be further optimized by using alternative lipid compositions, surface modifications or encapsulation techniques, and these could be investigated in the future to enhance the DL capacity, stability and controlled release properties.

In addition, the present cytological studies revealed that CDDP-PNA-Lip had significant antitumour effects after only 48 h of treatment, even at low concentrations. It was speculated that this phenomenon may be related to the antitumour mechanism of CDDP, which is activated by replacing one of the chlorine ligands with a water ligand once the agent enters the cell because water is a better leaving group than chlorine (the core of CDDP prefers to bind to chlorine), and because the concentration of chlorine ions in the cytoplasm is relatively low (4-20 mM). The pretreatment approach adopted in the present study resulted in the activation of liposome-encapsulated CDDP, which could exert its antitumour effect faster and more efficiently compared to direct CDDP use. Moreover, after an intravenous injection of CDDP in sterile saline via the conventional mode of administration, 65-95% of CDDP can bind to plasma proteins and lead to its inactivation within 24 h of administration due to the relatively high concentration of chloride (100 nM) in the blood (45). The present study was able to protect CDDP from high chloride concentrations and plasma proteins, and improve drug utilization after its encapsulation in liposomes. In the experiments using mice, the CDDP-PNA-Lip combination had a tumour inhibition rate of 83.1% when only 2.5 mg/kg CDDP was used (~50% of the standard dose), which was 2.65 times higher than that of the CDDP group and 1.63 times greater than that of the CDDP-Lip group. Compared with other studies, a stronger tumour-suppressive effect was achieved using only 50% of the CDDP dose in the same time period.

In the *in vitro* experiments, A549 cells showed an increase in apoptotic rate in response to CDDP-PNA-Lip compared with CDDP and CDDP-Lip; however, H460 cells showed a decrease in apoptotic rate in response to CDDP-Lip and CDDP-PNA-Lip compared with CDDP. This difference may be attributed to the variances in cellular uptake mechanisms of free and liposomal drugs. Free CDDP is primarily absorbed by cells through passive diffusion, which is greatly influenced by the drug concentration. By contrast, as shown in our previous study (23), the liposomes were internalized via receptor-mediated endocytosis. However, it is important to note that different cells may demonstrate alternate uptake efficiencies. The varying uptake efficiencies of cells for liposomal drugs may have contributed to this situation. Consequently, the effectiveness of the drug may be reduced, leading to this phenomenon. However, it was demonstrated through small animal imaging that the use of liposome-encapsulated drugs may effectively concentrate the drug at the tumour site compared with the free drug. The drug concentration at the tumour site was shown to remain significantly higher than that of the free drug until the drug was fully metabolized. This process does not affect the application of CDDP. Notably, the use of only A549 and H460 cell lines is a limitation of the present study and further NSCLC cell lines, as well as MUC1-positive and MUC1-negative cells, should be used in the future to investigate the specificity of the targeting mechanism.

In addition, the CDDP-Lip targeting MUC1 constructed in the present study hold promise for application in other types of cancer or disease. Platinum-based compounds are currently the most commonly used chemotherapeutic agents in clinical practice. They are employed as first-line treatment for a wide range of malignant tumours or as alternative therapies following the development of resistance to the initial chemotherapeutic agent. For example, in addition to NSCLC, CDDP is widely used in treating solid tumours, including melanoma, breast cancer, colon cancer and liver cancer (46). In addition, the target site of choice, MUC1, is a mucin widely expressed in a variety of malignant tumours. The MUC1 antigenic epitopes expressed on the surface of malignant tumours are exposed due to alterations in their glycosylation levels. This makes the targeting of MUC1 even more conducive to reducing non-tumour site-specific release. For example, in the study by Li *et al* (47), the expression of MUC1 was revealed to be significantly upregulated in breast cancer. As CDDP is a commonly used drug for breast cancer, developing CDDP liposomes that can target MUC1 is expected to enable drug-targeted delivery to patients with breast cancer and high MUC1 expression. Furthermore, our previous studies have demonstrated the targeting of the generated liposomes to hepatocellular carcinoma and colorectal cancer (23,33). It is expected that targeted CDDP can be delivered to patients with these types of cancer using our specialized nanodelivery system. In addition, CDDP shows good clinical synergy with gemcitabine and pemetrexed; the gemcitabine/CDDP regimen has been extensively evaluated in Phase II and Phase III randomized trials in advanced NSCLC, with response rates ranging from 21 to 40%, and a median survival of ~9 months (48). Additionally, in a study by Cui *et al* (49), the combination of farnesyltamol and CDDP successfully inhibited the progression of NSCLC by targeting the DUSP26-mediated signalling pathway, suggesting potential clinical applications of NSCLC.

CDDP is widely used to treat various types of malignant tumours. For example, it has shown synergistic antitumour effects with temozolomide (TMZ) in several clinical studies (50,51), such as in the treatment of advanced malignant melanoma (50). TMZ creates methyl adducts at the 0.6 position of guanine, while CDDP can reduce the activity of the DNA repair enzyme AGAT, which inhibits the formation of methyl adducts, thereby boosting the antitumour effects of TMZ (52). The chosen target, MUC1, is a tumour-specific protein found extensively on the surface of various malignant tumours. Targeting MUC1 has also been proven to be effective in studies of other types of malignant tumours. HuMNC2-CAR44 CAR-T cells are being utilized in a clinical trial (NCT04020575; classic.

clinicaltrials.gov/ct2/show/NCT04020575) to treat metastatic breast cancer, which is currently enrolling participants. In another clinical study (NCT02544880; classic.clinicaltrials.gov/ct2/show/NCT02544880), researchers assessed the safety and immunological effectiveness of tadalafil combined with an antitumour vaccine containing MUC1 and poly(ICLC); this study revealed that tadalafil had a beneficial immunomodulatory effect on patients with recurrent primary squamous cell carcinoma of the head and neck. In addition, the antitumour vaccine MUC1/polyICLC can be used as an adjuvant to tadalafil therapy in primary head and neck squamous cell carcinoma (53).

In conjunction with our previous studies, it may be hypothesized that in addition to pre-preparation of CDDP, which enables it to better exert its effects on organisms, the enhanced antitumour effect may also be due to liposomes assisting in the intracellular delivery of CDDP. In addition to passive diffusion, the transport efficiency of CDDP is influenced by copper transporter protein 1 (CTR1), which is crucial for the internalization of CDDP in tumour cells (54). Several *in vitro* and *in vivo* studies (55,56) have shown that CDDP resistance in cancer is associated with changes in the levels of CTR1 (55). Differences in the efficacy of CDDP therapy and the development of resistance between different types of cancer or individuals may also be associated with the activity of CTR1. We previously reported that PNA-Lip can be generated through lattice protein-mediated endocytosis, this explains the mechanism by which liposomes were endocytosed by cells in this study (57,58). Furthermore, we revealed that tumour cells express a significant amount of MUC1 on their surface (23). This property allows for unrestricted transport of CDDP into the cell without having to receive the rate limitation of CRT1 transport as is the case with direct CDDP, allowing for more effective targeting of tumours.

The CDDP-PNA-Lip prepared in the present study were revealed to have a significant anti-NSCLC effect, and by adding DPPG to the liposome formulation, the stability and DL capacity of the liposomes were better than those of traditional liposomes. However, the present study has several limitations. First, the cytotoxicity of CDDP after pretreatment was tested, and the cytotoxicity of CDDP did not differ significantly before and after treatment, but other characteristics were not detected, such as its integration capacity with DDTC. Another limitation of this study is that CDDP is mainly administered intravenously in clinical practice, whereas the present study used intraperitoneal injection. Although studies have shown that small molecules with a particle size <300 nm can produce therapeutic effects comparable to those of intravenous injection when administered intraperitoneally, some variability still exists that hinders the complete replication of the therapeutic effects of intravenous injection. At present, this process must be considered when advancing clinical trials to determine whether pretreatment with CDDP may result in unforeseen toxic side effects, necessitating further toxicological analysis. The *in vivo* clearance of liposomes is also an issue that requires further attention. According to Ishida *et al* (59), the complement system serves a key role in enhancing the clearance of liposomes when they are negatively charged and relatively large in size. Therefore, constructing smaller liposomes may offer an effective solution to this issue. In addition, there may be some variability between the two cell lines used in the present study. Although the ability of PNA to target MUC1 was shown in our previous study (33), a more systematic approach may be warranted in future studies. This could involve isolating primary cells from patients or constructing MUC1-overexpressing cell lines using a lentivirus. This step is necessary to clarify the specificity of the targeting mechanism and to assess the potential toxicity of the formulation to normal lung cell lines.

In conclusion, in the present study, CDDP-loaded ligand-modified liposomes were successfully prepared; these materials were well characterized and stable, suggesting that they could be used for the delivery of CDDP *in vivo*. This approach effectively improved the time of CDDP in animals and increased the local drug concentration and residence time at the tumour site through targeting. *In vitro* experiments proved that CDDP-PNA-Lip had a significant inhibitory effect on tumour cells. Therefore, the present study is highly important for evaluating the clinical application of CDDP, improving the antitumour efficacy of drugs and reducing the administration dose, and indicated that CDDP-loaded ligand-modified liposomes may be used as a potential treatment for NSCLC.

Acknowledgements

Not applicable.

Funding

This research was funded by The Natural Science Foundation of Shandong Province, (grant no. ZR20180709017), the National Natural Science Foundation of China, (grant nos. 82070856, 81274093 and 81871892) and the Weifang City Science and Technology Project Plan (grant no. 2022YX038).

Availability of data and materials

The data generated in the present study may be requested from the corresponding author.

Authors' contributions

ZG performed conceptual design. WY conducted methodology and performed experiments. The data were quantified and analysed by RK, FW and MS. LW, SZ and JW performed bioinformatics analyses. FY and MQ examined the physiological indicators of the animals. SS, AW and HW conducted animal experiments. YiW and YuW supervised and participated in the cell experiments. YiW, YuW and BY wrote the original manuscript. ZG and BY reviewed and edited the article, supervised by ZG. ZG was responsible for project management. ZG, WY and MQ obtained funds. ZG and WY confirming the authenticity of all the raw data. All authors read and approved the final version of the manuscript.

Ethics approval and consent to participate

The animal experimental protocol used in the present study was approved by the Ethical Review Committee of Shandong Second Medical University.

Patient consent for publication

Not applicable.

Competing interests

The authors declare that they have no competing interests.

Use of artificial intelligence tools

During the preparation of this work, AI tools were used to improve the readability and language of the manuscript or to generate images, and subsequently, the authors revised and edited the content produced by the AI tools as necessary, taking full responsibility for the ultimate content of the present manuscript.

References

1. Noordeldeen R and Bach H: Current and future development in lung cancer diagnosis. Int J Mol Sci 22: 8661, 2021.
2. Wu F, Wang L and Zhou C: Lung cancer in China: Current and prospect. Curr Opin Oncol 33: 40-46, 2021.
3. Teramoto K, Ozaki Y, Hanaoka J, Sawai S, Tezuka N, Fujino S, Daigo Y and Kontani K: Predictive biomarkers and effectiveness of MUC1-targeted dendritic-cell-based vaccine in patients with refractory non-small cell lung cancer. Ther Adv Med Oncol 9: 147-157, 2017.
4. Sun M, Shi Y, Dang UJ and Di Pasqua AJ: Phenethyl isothiocyanate and cisplatin co-encapsulated in a liposomal nanoparticle for treatment of non-small cell lung cancer. Molecules 24: 801, 2019.
5. Wang Y, Qian J, Yang M, Xu W, Wang J, Hou G, Ji L and Suo A: Doxorubicin/cisplatin co-loaded hyaluronic acid/chitosan-based nanoparticles for in vitro synergistic combination chemotherapy of breast cancer. Carbohydr Polym 225: 115206, 2019.
6. Nasrollahi F, Koh YR, Chen P, Varshosaz J, Khodadadi AA and Lim S: Targeting graphene quantum dots to epidermal growth factor receptor for delivery of cisplatin and cellular imaging. Mater Sci Eng C Mater Biol Appl 94: 247-257, 2019.
7. Gualdani R, de Clippele M, Ratbi I, Gailly P and Tajeddine N: Store-operated calcium entry contributes to cisplatin-induced cell death in non-small cell lung carcinoma. Cancers (Basel) 11: 430, 2019.
8. Ashique S, Sandhu NK, Chawla V and Chawla PA: Targeted drug delivery: Trends and perspectives. Curr Drug Deliv 18: 1435-1455, 2021.
9. Tavakkoli Yaraki M, Daqiqeh Rezaei S and Tan YN: Simulation guided design of silver nanostructures for plasmon-enhanced fluorescence, singlet oxygen generation and SERS applications. Phys Chem Chem Phys 22: 5673-5687, 2020.
10. Sarfaraz N and Khan I: Plasmonic gold nanoparticles (AuNPs): Properties, synthesis and their advanced energy, environmental and biomedical applications. Chem Asian J 16: 720-742, 2021.
11. Mittal D, Singh A, Kohli K and Verma AK: Engineering biosafe cisplatin loaded nanostructured lipid carrier: Optimisation, synthesis, pharmacokinetics and biodistribution. J Microencapsul 39: 522-538, 2022.
12. Herrera-Juarez M, Serrano-Gomez C, Bote-de-Cabo H and Paz-Ares L: Targeted therapy for lung cancer: Beyond EGFR and ALK. Cancer 129: 1803-1820, 2023.
13. Moosavian SA, Abnous K, Akhtari J, Arabi L, Gholamzade Dewin A and Jafari M: 5TR1 aptamer-PEGylated liposomal doxorubicin enhances cellular uptake and suppresses tumour growth by targeting MUC1 on the surface of cancer cells. Artif Cells Nanomed Biotechnol 46: 2054-2065, 2018.
14. Noble GT, Stefanick JF, Ashley JD, Kiziltepe T and Bilgicer B: Ligand-targeted liposome design: Challenges and fundamental considerations. Trends Biotechnol 32: 32-45, 2014.
15. Filipczak N, Pan J, Yalamarty SSK and Torchilin VP: Recent advancements in liposome technology. Adv Drug Deliv Rev 156: 4-22, 2020.
16. Saw PE, Park J, Lee E, Ahn S, Lee J, Kim H, Kim J, Choi M, Farokhzad OC and Jon S: Effect of PEG pairing on the efficiency of cancer-targeting liposomes. Theranostics 5: 746-754, 2015.
17. Underwood C, van Eps AW, Ross MW, Laverman P, van Bloois L, Storm G and Schaer TP: Intravenous technetium-99m labelled PEG-liposomes in horses: A safety and biodistribution study. Equine Vet J 44: 196-202, 2012.
18. Namba M, Hattori N, Hamada H, Yamaguchi K, Okamoto Y, Nakashima T, Masuda T, Sakamoto S, Horimasu Y, Miyamoto S, *et al*: Anti-KL-6/MUC1 monoclonal antibody reverses resistance to trastuzumab-mediated antibody-dependent cell-mediated cytotoxicity by capping MUC1. Cancer Lett 442: 31-39, 2019.
19. Bouillez A, Adeegbe D, Jin C, Hu X, Tagde A, Alam M, Rajabi H, Wong KK and Kufe D: MUC1-C promotes the suppressive immune microenvironment in non-small cell lung cancer. Oncoimmunology 6: e1338998, 2017.
20. Kumar P, Lindberg L, Thirkill TL, Ji JW, Martsching L and Douglas GC: The MUC1 extracellular domain subunit is found in nuclear speckles and associates with spliceosomes. PLoS One 7: e42712, 2012.
21. Beack S, Cho M, Kim YE, Ahn GO and Hahn SK: Hyaluronate-peanut agglutinin conjugates for target-specific bioimaging of colon cancer. Bioconjug Chem 28: 1434-1442, 2017.
22. Wu X, McFall-Boegeman H, Rashidijahanabad Z, Liu K, Pett C, Yu J, Schorlemer M, Ramadan S, Behren S, Westerlind U and Huang X: Synthesis and immunological evaluation of the unnatural β-linked mucin-1 Thomsen-Friedenreich conjugate. Org Biomol Chem 19: 2448-2455, 2021.
23. Li X, Diao W, Xue H, Wu F, Wang W, Jiang B, Bai J, Lian B, Feng W, Sun T, *et al*: Improved efficacy of doxorubicin delivery by a novel dual-ligand-modified liposome in hepatocellular carcinoma. Cancer Lett 489: 163-173, 2020.
24. Zahednezhad F, Zakeri-Milani P, Shahbazi Mojarrad J and Valizadeh H: The latest advances of cisplatin liposomal formulations: essentials for preparation and analysis. Expert Opin Drug Deliv 17: 523-541, 2020.
25. Long DF and Repta AJ: Cisplatin: Chemistry, distribution and biotransformation. Biopharm Drug Dispos 2: 1-16, 1981.
26. Cheng Y, Zhao P, Wu S, Yang T, Chen Y, Zhang X, He C, Zheng C, Li K, Ma X and Xiang G: Cisplatin and curcumin co-loaded nano-liposomes for the treatment of hepatocellular carcinoma. Int J Pharm 545: 261-273, 2018.
27. Saracchini S, Foltran L, Tuccia F, Bassini A, Sulfaro S, Micheli E, Del Conte A, Bertola M, Gion M, Lorenzon M and Tumolo S: Phase II study of liposome-encapsulated doxorubicin plus cyclophosphamide, followed by sequential trastuzumab plus docetaxel as primary systemic therapy for breast cancer patients with HER2 overexpression or amplification. Breast 22: 1101-1107, 2013.
28. Wang H, Wu H, Shen H, Geng S, Wang B, Wang Y, Ma X, Li G and Tan M: A bimodal MRI and NIR liposome nanoprobe for tumor targeted molecular imaging. J Mater Chem B 3: 8832-8841, 2015.
29. Theodosiou M, Sakellis E, Boukos N, Kusigerski V, Kalska-Szostko B and Efthimiadou E: Iron oxide nanoflowers encapsulated in thermosensitive fluorescent liposomes for hyperthermia treatment of lung adenocarcinoma. Sci Rep 12: 8697, 2022.
30. Zhang X, Lü S, Han J, Sun S, Wang L and Li Y: Preparation, characterization and in vivo distribution of solid lipid nanoparticles loaded with syringopicroside. Pharmazie 66: 404-407, 2011.
31. Lippard SJ: New chemistry of an old molecule: Cis-[Pt(NH3)2Cl2]. Science 218: 1075-1082, 1982.
32. Newman MS, Colbern GT, Working PK, Engbers C and Amantea MA: Comparative pharmacokinetics, tissue distribution, and therapeutic effectiveness of cisplatin encapsulated in long-circulating, pegylated liposomes (SPI-077) in tumor-bearing mice. Cancer Chemother Pharmacol 43: 1-7, 1999.
33. Diao W, Yang B, Sun S, Wang A, Kou R, Ge Q, Shi M, Lian B, Sun T, Wu J, *et al*: PNA-modified liposomes improve the delivery efficacy of CAPIRI for the synergistic treatment of colorectal cancer. Front Pharmacol 13: 893151, 2022.
34. Bar J, Ofek E, Barshack I, Gottfried T, Zadok O, Kamer I, Urban D, Perelman M and Onn A: Transformation to small cell lung cancer as a mechanism of resistance to immunotherapy in non-small cell lung cancer. Lung Cancer 138: 109-115, 2019.
35. Ettinger DS, Wood DE, Aisner DL, Akerley W, Bauman JR, Bharat A, Bruno DS, Chang JY, Chirieac LR, D'Amico TA, *et al*: Non-small cell lung cancer, version 3.2022, NCCN clinical practice guidelines in oncology. J Natl Compr Canc Netw 20: 497-530, 2022.

36. Riaz SP, Lüchtenborg M, Coupland VH, Spicer J, Peake MD and Møller H: Trends in incidence of small cell lung cancer and all lung cancer. Lung Cancer 75: 280-284, 2012.
37. Zhong WZ, Yan HH, Chen KN, Chen C, Gu CD, Wang J, Yang XN, Mao WM, Wang Q, Qiao GB, *et al*: Erlotinib versus gemcitabine plus cisplatin as neoadjuvant treatment of stage IIIA-N2 EGFR-mutant non-small-cell lung cancer: Final overall survival analysis of the EMERGING-CTONG 1103 randomised phase II trial. Signal Transduct Target Ther 8: 76, 2023.
38. Stinchcombe TE: Flashback foreword: Cisplatin/pemetrexed in non-small-cell lung cancer. J Clin Oncol 41: 2455-2456, 2023.
39. Makwana V, Karanjia J, Haselhorst T, Anoopkumar-Dukie S and Rudrawar S: Liposomal doxorubicin as targeted delivery platform: Current trends in surface functionalization. Int J Pharm 593: 120117, 2021.
40. Lozano N, Al-Ahmady ZS, Beziere NS, Ntziachristos V and Kostarelos K: Monoclonal antibody-targeted PEGylated liposome-ICG encapsulating doxorubicin as a potential theranostic agent. Int J Pharm 482: 2-10, 2015.
41. Kim DM, Kim M, Park HB, Kim KS and Kim DE: Anti-MUC1/CD44 dual-aptamer-conjugated liposomes for cotargeting breast cancer cells and cancer stem cells. ACS Appl Bio Mater 2: 4622-4633, 2019.
42. Panchamoorthy G, Jin C, Raina D, Bharti A, Yamamoto M, Adeebge D, Zhao Q, Bronson R, Jiang S, Li L, *et al*: Targeting the human MUC1-C oncoprotein with an antibody-drug conjugate. JCI Insight 3: e99880, 2018.
43. Ranjbar-Navazi Z, Fathi M, Abdolahinia ED, Omidi Y and Davaran S: MUC-1 aptamer conjugated InP/ZnS quantum dots/nanohydrogel fluorescent composite for mitochondria-mediated apoptosis in MCF-7 cells. Mater Sci Eng C Mater Biol Appl 118: 111469, 2021.
44. Marzban E, Alavizadeh SH, Ghiadi M, Khoshangosht M, Khashayarmanesh Z, Abbasi A and Jaafari MR: Optimizing the therapeutic efficacy of cisplatin PEGylated liposomes via incorporation of different DPPG ratios: In vitro and in vivo studies. Colloids Surf B Biointerfaces 136: 885-891, 2015.
45. Zia MK, Siddiqui T, Ali SS, Rehman AA, Ahsan H and Khan FH: Chemotherapeutic drugs and plasma proteins: Exploring new dimensions. Curr Protein Pept Sci 19: 937-947, 2018.
46. Romani AMP: Cisplatin in cancer treatment. Biochem Pharmacol 206: 115323, 2022.
47. Li Z, Yang D, Guo T and Lin M: Advances in MUC1-mediated breast cancer immunotherapy. Biomolecules 12: 952, 2022.
48. Crinò L, Calandri C, Maestri A and Marrocolo F: Gemcitabine and cisplatin combination in early-stage non-small-cell lung cancer. Oncology (Williston Park) 15 (3 Suppl 6): S40-S42, 2001.
49. Cui Z, Li D, Zhao J and Chen K: Falnidamol and cisplatin combinational treatment inhibits non-small cell lung cancer (NSCLC) by targeting DUSP26-mediated signal pathways. Free Radic Biol Med 183: 106-124, 2022.
50. Daponte A, Ascierto PA, Gravina A, Melucci M, Scala S, Ottaiano A, Simeone E, Palmieris G and Comella G: Temozolomide and cisplatin in avdanced malignant melanoma. Anticancer Res 25: 1441-1447, 2005.
51. Christodoulou C, Bafaloukos D, Linardou H, Aravantinos G, Bamias A, Carina M, Klouvas G and Skarlos D; Hellenic Cooperative Oncology Group: Temozolomide (TMZ) combined with cisplatin (CDDP) in patients with brain metastases from solid tumors: A hellenic cooperative oncology group (HeCOG) phase II study. J Neurooncol 71: 61-65, 2005.
52. Bafaloukos D, Tsoutsos D, Kalofonos H, Chalkidou S, Panagiotou P, Linardou E, Briassoulis E, Efstathiou E, Polyzos A and Fountzilas G,: Temozolomide and cisplatin versus temozolomide in patients with advanced melanoma: A randomized phase II study of the Hellenic cooperative oncology group. Ann Oncol 16: 950-957, 2005.
53. Weed DT, Zilio S, Reis IM, Sargi Z, Abouyared M, Gomez-Fernandez CR, Civantos FJ, Rodriguez CP and Serafini P: The reversal of immune exclusion mediated by tadalafil and an anti-tumor vaccine also induces PDL1 Upregulation in recurrent head and neck squamous cell carcinoma: interim analysis of a phase I clinical trial. Front Immunol 10: 1206, 2019.
54. Ishida S, Lee J, Thiele DJ and Herskowitz I: Uptake of the anticancer drug cisplatin mediated by the copper transporter Ctr1 in yeast and mammals. Proc Natl Acad Sci USA 99: 14298-14302, 2002.
55. Akhter J, Goswami P, Ali Beg MM, Ahmad S, Najmi AK and Raisuddin S: Protective effect of rosmarinic acid on the transmembrane transporter Ctr1 expression in cisplatin-treated mice. J Cancer Res Ther 19: 1753-1759, 2023.
56. Huang CP, Fofana M, Chan J, Chang CJ and Howell SB: Copper transporter 2 regulates intracellular copper and sensitivity to cisplatin. Metallomics 6: 654-661, 2014.
57. Akerfeldt MC, Tran CMN, Shen C, Hambley TW and New EJ: Interactions of cisplatin and the copper transporter CTR1 in human colon cancer cells. J Biol Inorg Chem 22: 765-774, 2017.
58. Zhang P, Li B, Chen Q, Wang H and Feng Q: Glucose restriction induces ROS-AMPK-mediated CTR1 expression and increases cisplatin efficiency in NSCLC. Cancer Lett 543: 215793, 2022.
59. Ishida T, Harashima H and Kiwada H: Liposome clearance. Biosci Rep 22: 197-224, 2002.